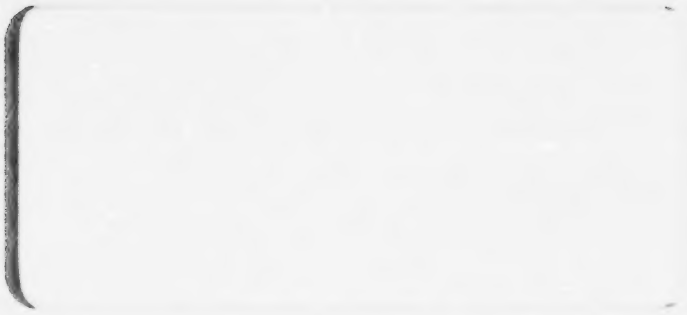

**Nova Scotia Research Foundation Corporation**
**Dartmouth, Nova Scotia**

CONTRACT SERIAL NO. ISQ85-00183

CONTRACTOR: Nova Scotia
Research Foundation
Corporation

Requisition no. 23440-5-9183

# DEVELOPMENT OF ENGINEERING CERAMICS HAVING HIGH TOUGHNESS, THERMAL SHOCK AND EROSION RESISTANCE

by

H. A. Kazi, Ph.D., P.Eng.

Submitted to

Mr. K. E. Bell
Energy Mines and Resources
CANMET, Mineral Science Laboratories
555 Booth St.
Ottawa, Ontario

On Fulfillment of Contract
DSS 03SQ.23440-5-9183

July 20, 1986

62 pp

MICROMEDIA

NOVA SCOTIA RESEARCH FOUNDATION CORPORATION
P.O. Box 790, Dartmouth, Nova Scotia, Canada, B2Y 3Z7
Tel: (902) 424-8670
Telex 019 - 22719

## TABLE OF CONTENTS


| | | PAGE |
|---|---|---|
| | ABSTRACT | v |
| 1. | INTRODUCTION AND OBJECTIVES | 1 |
| 2. | EXPERIMENT AND PROCEDURES | 6 |
| 2.1 | Preparation of Samples | 6 |
| | 2.1.a Raw Materials Used | 6 |
| | 2.1.b Fabrication of Samples | 7 |
| 3. | EXAMINATION OF PROPERTIES | 10 |
| 3.1 | Shrinkage and Density Measurements | 10 |
| 3.2 | Microstructural Examination and Results | 12 |
| 3.3 | Hardness Measurements | 20 |
| 3.4 | Determination of Erosion Resistance | 20 |
| | 3.4.a Procedure | 20 |
| | 3.4.b Erosion Test Results | 22 |
| 3.5 | Thermal Shock Measurements and Results | 22 |
| | 3.5.a Procedure | 22 |
| | 3.5.b Thermal Shock Test Results | 25 |
| 3.6 | Fracture Toughness Measurements | 37 |
| | 3.6.a Procedure | 37 |
| | 3.6.b Fracture Toughness Results | 39 |
| 4. | DISCUSSION | 41 |
| 5. | CONCLUSIONS | 47 |

## TABLE OF CONTENTS (Continued)


| | PAGE |
|---|---|
| ACKNOWLEDGMENTS | 49 |
| REFERENCES | 50 |
| APPENDIX A - PHYSICAL PROPERTIES OF POWDER | 52 |
| APPENDIX B - Photomicrographs of Sintered Samples | 57 |

## LIST OF TABLES


| | PAGE |
|---|---|
| TABLE 1 | 8 |
| TABLE 2 | 9 |
| TABLE 3 | 11 |
| TABLE 4 | 13 |
| TABLE 5 | 35 |
| TABLE 6 | 40 |

## LIST OF FIGURES


| | | PAGE |
|---|---|---|
| Figure 1 | | 14 |
| Figure 2 | | 15 |
| Figure 3 | | 16 |
| Figure 4 | | 17 |
| Figure 5 | | 18 |
| Figure 6 | | 19 |
| Figure 7 | Schematic of Abrasive Test Apparatus | 21 |
| Figure 8 | Schematic Diagram of Thermal Shock Test Apparatus | 23 |
| Figure 9 | Failure Zone Plot of Sample A1 | 26 |
| Figure 10 | Failure Zone Plot of Sample A2 | 27 |
| Figure 11 | Failure Zone Plot of Sample B1 | 28 |
| Figure 12 | Failure Zone Plot of Sample B3 | 29 |
| Figure 13 | Failure Zone Plot of Sample C1 | 30 |
| Figure 14 | Failure Zone Plot of Sample C2 | 31 |
| Figure 15 | Failure Zone Plot of Sample D1 | 32 |
| Figure 16 | Failure Zone Plot of Sample D2 | 33 |
| Figure 17 | Failure Zone Plot of Sample E2 | 34 |
| Figure 18 | Single Edge Notched Bend Specimen | 36 |
| Figure 19 | Testing of a Fracture Toughness Specimen | 38 |
| Figure 20 | Hardness Vs % Theoretical Density | 42 |
| Figure 21 | % Theoretical Density Vs Erosion Rate | 43 |
| Figure 22 | Hardness Vs Erosion Rate | 44 |

## ABSTRACT

Alumina and alumina particulate composite samples, made of fine (alumina; ∿ 0.5 U and 0.92 U) powders of various purity and fine-grained stabilized zirconia, were prepared by both slipcasting and isostatic pressing methods. All these specimens were tested for abrasion, thermal shock resistance, and fracture toughness, as well as hardness, density and microstructure. The procedure for sample preparation and test methods are described.

Overall it was found that the physical properties of Alcoa-16 + 5% $ZrO_2$ were better than that of Alcoa-39 + 5% $ZrO_2$. Specifically, the fracture toughness of Alcoa-16, the least expensive powder at less than \$1/lb, + 5% $ZrO_2$ was superior to that of the more expensive powders RC-HB-DBM, \$14/lb, + 5% $ZrO_2$[19] and Alcoa-39, \$12/lb, + 5% $ZrO_2$ produced under conditions practical in this study.

---

Les échantillons d'alumine et d'alumine de particules composé fait de poudre fine (0.55 U et 0.92 U) de pureté varié et de fine granules de zirconia stabilize on été préparé par les methodes de coulée a'l'engobe et de pressage-isostatic. Les spécimens ont été mesuré pour la résistance au choc thermique, la resistance a'l'érosion, la resistance aux fractures et la durete, la densité, et la grosseur de granules. Le procedure pour la préparation des échantillons et la methode d'essaie sont décrite.

Il a été determine que les caractéristiques physiques de L'alcoa-16 + 5% $ZrO_2$ ont été meilleur que L'alcoa-39 + 5% $ZrO_2$, et comparable au RC-HB-DBM + 5% $ZrO_2$. Spécifiquement la résistance aux fractures de L'alcoa-16 + 5% $ZrO_2$ la poudre la moins dispendieuse, a été superieur aux poudres les plus dispendieuses RC-HB-DBM, et alcoa-39 + 5% $ZrO_2$ produites sous les conditions de cette étude.

## 1. INTRODUCTION AND OBJECTIVES

The exciting properties of ceramics include strength at higher temperature, wear resistance, hardness, stiffness, corrosion resistance, and relatively low density. They can provide lower operating costs due to longer service life and reduced down time in critical environments. Inherent brittleness and low thermal shock resistance are two properties of ceramics that need improvement. The strength of a material against brittle fracture depends on the size of the faults that are present in the material and the material's own fracture toughness.

Any variability in fault size from one component to another results in variability in their strength. Ceramic production must therefore be precisely reproducible and free from fault-producing accidents such as those that can result from unclean processing conditions, uneven distribution of impurities or catalysts and uneven internal stresses. High strength material therefore can be produced by improved processing and/or with toughening mechanisms to increase the energy requirement for crack extension. Particles of zirconium oxide have been known to increase the strength of aluminum oxide in which they are embedded.(1) In the solid state sintering, the powder consists of individual crystals which remain solid throughout the heat treatment.

The system is heated to temperatures where diffusion of the atoms in the solid state can occur; atom movement can then reduce the surface energy of the system either by densification - movement of atoms from the grain boundary region of the solid/gas interface - or by coarsening - movement of atoms between different regions on the solid/gas interface. Densification reduces the distance between particle centres, so the component shrinks, lowering porosity. The coarsening process, in contrast, wastes the surface energy which provides the driving force for densification without changing the porosity. These processes can be speeded up by higher sintering temperatures and by very fine particles (shorter diffusion distance) of sub-micrometer size.

An attractive aid to densification is to use an additive which acts without forming a liquid phase at the boundaries; trace additions of magnesium oxide work in this way for aluminum oxide. Another recognized problem is that conventional firing can yield results only as uniform as the quality of the powder compact (green sample). If severe variations in packing density occur in the compact, then corresponding inhomogeneties and faults will occur in the finished product.

Particle size distribution of powders is known to have a great influence on the sintered density of ceramics which in turn might have an influence on the properties of final products. It is a recognized fact that strength and thermal shock resistance of ceramic composites can be improved if particle sizes are kept sufficiently small.

Erosion has been encountered and has caused severe problems in a number of prototype plants used to evaluate coal liquefaction and gasification processes. Analysis of the causes of these problems and of available engineering systems solutions has shown that, in many cases, the rate of loss can be reduced to acceptable levels by careful attention to process control, component design, and materials selection. Nevertheless, some areas of recurring erosion problems are likely to remain, especially in the areas of raw material preparation and handling, and in effluent handling and disposal systems. Components such as valves and pumps are probably the most critically affected because of their importance to process control and safety, and because they are high cost items. Some areas of the associated piping, especially bends, and solids clean-up equipment such as cyclones and hydrocyclones may also be included in this category, but are more amenable to maintenance. Such critical areas can usually justify the application of the most erosion-resistant materials available, which are ceramics.

The materials problems involved in commercial coal preparation plants involve essentially erosive and abrasive wear from coal particles and the associated mineral content. Pumps handling coal

slurries are run at reduced velocities and employ hardened alloy internals; valves for such service usually employ hardened alloys for the critical areas and often embody design features to remove or isolate seals from contact with the slurry.

Higher thermal shock resistance and erosion resistance ceramic inserts are required for use in nozzles to burn coal-water-mixtures.

Ceramics are now being treated and used to replace traditional materials in many oil drilling applications. The handling of drilling muds is an example of ceramics extending service life and reducing operating costs. Simulated mud pumpline tests of shrunk fit high alumina liners has shown promising results. Actual field tests have shown that unprotected ceramic mud nozzles last as long as tungsten carbide nozzles if they are not broken during installation.

The microstructure of a finished ceramic, hence its properties, are very dependent on the fabrication procedure used. Common fabrication routes include hot-pressing, sintering, reaction-bonding and hot isostatic pressing, each of which may be applied to a given ceramic, and can produce in the finished product quite different structures and properties. While ceramic materials have potential for higher hardness, hence higher erosion resistance (if they erode by a transgranular mechanism) than metals, the actual trends in behaviour are not simple nor very well understood. As a class of materials, ceramics will not attain wide engineering acceptance unless higher levels of fracture toughness can be developed. Research programs underway on ceramic matrix composites, and on transformation-toughened ceramics are aimed in this direction.

Ceramic composites expand the range of applicability by increasing the diverse properties we can achieve, particularly the increase in strength of fracture toughness. Such resistance is important since it determines mechanical reliability.

A successful technique for producing stronger and tougher ceramics makes use of stress-induced phase transformation in $ZrO_2$ from the teragonal phase, which is metastable at room temperature, to monoclinic phase. The transformation is athermal and diffusionless and involves a shear deformation and a 3% to 5% increase in volume.[2-4] The retained tetragonal phase is thought to transform to monoclinic phase under the elevated stress at the running crack tip. During this process, part of the energy that would otherwise be available for crack formation is absorbed, resulting in a higher toughness for the composite material.[5,6] Significant improvements in fracture toughness and flexural strength have been reported in $Al_2O_3$-x$ZrO_2$ system, as compared with the values of pure $Al_2O_3$.[7] The increase in fracture toughness of such systems (e.g. $Al_2O_3$-$ZrO_2$) depends on the morphology and distribution of $ZrO_2$ particles - their size, shape, concentration, and location in $Al_2O_3$ matrix, which are critically influenced by the processing methodology (e.g. mixing, consolidation, oil firing).[8-10]

The amount of toughening agent, tetragonal $ZrO_2$, can be fabricated by the addition of $Y_2O_3$ and by sintering. As shown in the $ZrO_2$-$Y_2O_3$ binary system,[11-13] $Y_2O_3$ forms a solid solution with $ZrO_2$ to reduce the t - m transformation temperature from 1200°C for pure $ZrO_2$ to ∿ 600°C for eutectoid composition containing ∿ 3-5 mol % $Y_2O_3$.

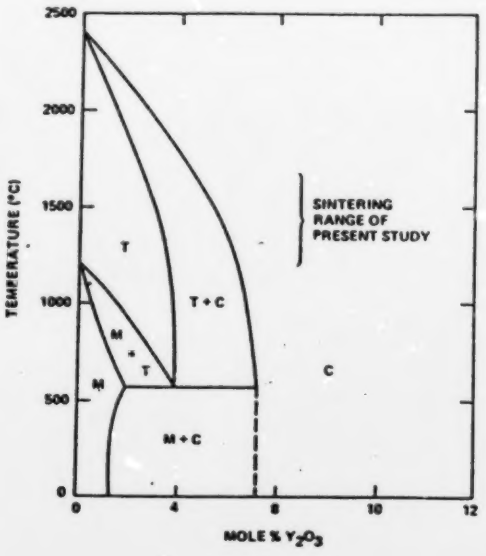

The critical inclusion size required to retain the $ZrO_2$ in its tetragonal state depends on the amount and type of alloy additions (e.g. $Y_2O_3$), the elastic modulus of the constraining matrix, and temperature in question.

The thermal shock resistance of sintered sample produced from 12 day ball milling (NORTON 100F) $Al_2O_3$ powder (particle size $\sim$ 0.91) appeared better than the samples produced from Reynolds RC-HP-DBM[14] powder, but the erosion resistance and the density were lower. It is expected that through blending of these two powders an optimum distribution can be obtained for the production of ceramic bodies having high thermal shock and erosion resistance.

The aim of this study is to contribute towards the development of a simple process, using commercially available low cost fine alumina powders, for the production of ceramics with improved thermal shock and erosion resistance with increased toughness. This study includes the following:

a) Development and assessment of production techniques for the manufacture of alumina and particulate alumina ceramic composites by both the slipcasting and the cold isostatic pressure (CIP) method.
b) Influence of blending powders of two different particle sizes.
c) Influence of the addition of toughening agents (stabilized $ZrO_2$).

The objective of this study was to compare quantitatively a variety of particulate ceramic materials (produced in this study) in terms of erosion resistance, thermal shock resistance, fracture toughness, density, hardness and microstructures.

From this study we hope to identify an economical ceramic product with improved properties which ultimately may be commercially produced for use as a replacement part where conventional materials are not suitable.

## 2. EXPERIMENT AND PROCEDURE

### 2.1 Preparation of Samples

#### 2.1.a Raw Materials Used

A variety of ceramic materials were used in the work. Many are listed below. The current market values of these powders are also included.

| Powder | Price/lb $ | Median Size U | Purity |
|---|---|---|---|
| Reynold RC-HB-DBM $Al_2O_3$ (with 0.05%MgO) | 14 | 0.55 | 99.95 |
| Norton F100 Calcined $Al_2O_3$, Ball Milled 12 days | 1.49 | ∿0.92 | |
| Alumalox-39 $Al_2O_3$ | 12 | 0.50 | 99.90 |
| Realox A-16 | <1 | ∿0.55 | 99.70 |
| TSK-Zirconia TZ-3Y | 127 | Crystallite Size 240A° | 94.87 |

The physical properties of these powders are given in Appendix A.

Norton 100F powder (calcined $Al_2O_3$) was ground to pass 100 mesh (Norton 6, Worcester Mass.). This powder was further ground for twelve days in a ball mill using Burundum Roalox jars (4 liter capacity) charged with 1 kg of powder predried at 1000°C, 0.7 litre anhydrous ethanol, and 3 kg of 2.5 cm alumina grinding media.

The remainder of the powders were used as obtained.

Material TZ-3Y was $Y_2O_3$ stabilized zirconia.

### 2.1.b Fabrication of Samples

The composition of powders given in Table 1 was used to prepare samples by slipcasting or isostatic pressing followed by sintering. The required amount of powders ($Al_2O_3$; $ZrO_2$) were ball milled together in absolute ethanol for two hours to obtain a homogeneous mixture. The mixture was then dried and used to prepare samples. Both the pure powder and the composite were either slipcast at pH 3.8-4 into a powder mold, or pressed isostatically in rubber molds at 138 MPa. These green samples were presintered at 1000°C for 5 hours, and then machined to sizes suitable for testing the various properties. The fracture toughness samples were all prepared by slipcasting. All samples were sintered after machining at 1500°C for 2 or 16 hours.

For convenience, considering the range of variables studied the samples whose properties were studied were given the designations shown in Table 2.

Extreme care was taken to avoid any contamination. The slurries of different composition behaved slightly different. It was necessary to carefully adjust the pH for individual slurry and the fluid content to obtain a solid cast.

**TABLE 1**

**Identification of Composition**

| Designation | % $Al_2O_3$ | | | | % $ZrO_2$ |
|---|---|---|---|---|---|
| | RC-HP-DBM | NORTON | ALCOA 39 | ALCOA 16 | |
| A | 50 | 50 | - | - | - |
| B | 47.50 | 47.5 | - | - | 5 |
| C | - | - | 100 | - | - |
| D | - | - | 95 | - | 5 |
| E | - | - | - | 95 | 5 |

**TABLE 2**

**Identification of Samples**

**(All Samples were Sintered at 1500°C)**

| Designation | Composition | Method Of Preparation | Sintering Time |
|---|---|---|---|
| A1 | A | SC | 16 |
| A2 | A | CIP | 2 |
| B1 | B | SC | 16 |
| B2 | B | SC | 2 |
| B3 | B | CIP | 2 |
| C1 | C | SC | 16 |
| C2 | C | CIP | 2 |
| D1 | D | SC | 16 |
| D2 | D | CIP | 2 |
| E1 | E | SC | 2 |
| E2 | E | CIP | 2 |

SC = Slipcasting

CIP = Cold Isostatically Pressed

## 3. EXAMINATION OF PROPERTIES

### 3.1 Shrinkage and Density Measurements

Shrinkage and densities of samples listed in Table 2 were measured. The presintered samples were machined to sizes suitable for erosion and thermal shock tests. The measurements of these machined samples before and after final sintering were used to calculate the shrinkages. The densities were measured by liquid (Kerosene) displacement method. The results are presented in Table 3. The % theoretical densities are also included in this table. The data for these measurements are included in the appendices.

A "theoretical" value for the density of the composites was obtained from the weights of the powders used, making the assumption that the density of fully sintered alumina is 3.975, that of Zirconia (tetragonal) is 5.72 and that the components mix ideally.

The following observations were made:

(a) For all slipcast samples, the shrinkage was higher along the diameter compared to the shrinkage along the length.

(b) Isostatically pressed samples (CIP) showed very little difference in shrinkage among the different directions.

(c) The slipcast (SC) samples in general had smaller shrinkages than that of isostatically pressed samples.

(d) The sintered density of ceramics produced from A-39 and A-39 + 5% $ZrO_2$ powder was higher than the ceramics produced from A-16 or A-16 + 5% $ZrO_2$ powder.

TABLE 3

CERAMIC DENSITIES AND SHRINKAGES

| Sample | Method of Preparation | Sintering Time Hr. | % Shrinkage | | Sintered Density $g/cm^3$ | % Theoretical Density |
|---|---|---|---|---|---|---|
| | | | Diameter | Length | | |
| A1 | SC | 16 | 12.93 | 12.17 | 3.68 | 92.57 |
| A2 | CIP | 2 | 13.88 | 14.38 | 3.49 | 87.80 |
| B1 | SC | 16 | 15.81 | 14.09 | 3.75 | 92.20 |
| B2 | SC | 2 | 10.43 | 9.39 | 3.62 | 89.01 |
| B3 | CIP | 2 | 14.45 | 14.46 | 3.61 | 88.76 |
| C1 | SC | 16 | 12.68 | 10.81 | 3.93 | 98.87 |
| C2 | CIP | 2 | 16.12 | 16.45 | 3.87 | 97.36 |
| D1 | SC | 16 | 14.74 | 11.94 | 4.01 | 98.60 |
| D2 | CIP | 2 | 16.01 | 16.30 | 3.87 | 95.16 |
| E1 | SC | 2 | 11.89 | 11.21 | 3.89 | 95.65 |
| E2 | CIP | 2 | 16.70 | 16.85 | 3.94 | 96.88 |

## 3.2 Microstructural Examination and Results

Samples were prepared from each type of sintered samples for microstructural examination. One mm thick slice was cut from the sintered ceramic body with a diamond cut-off wheel. At least four small pieces from it were set in Fisher clear quick mount compound. Rough grinding was done on automatic (Leco VP-50) polisher with Di-Mar discs (diamond powder impregnated abrasive paper) of 240, 320 and 600 grit. Rough polishing of the mounted samples was done with diamond paste of different grades. The polishing was completed with 0.05 μ alumina slurry. One of the ceramic pieces was then taken out of the mount and etched in hot concentrated $H_3PO_4$ for 1-4 minutes. The etched sample was then examined by optical microscope to assess the quality of the sample.

Some times it was necessary to polish the mounted sample further and/or adjust the etching time to obtain a good optical micrograph. The idea of mounting four samples on the same mount was to avoid preparation time as the samples could not be polished unmounted and could not be etched mounted.

One sample from each type of ceramic listed in Table 2 was examined, photomicrographs taken and the grain sizes were measured from the micrographs. The results of the grain size measurements are given in Table 4 along with the erosion test results and hardness. The micrographs of some typical samples are given in Figure 1 to Figure 6.

The following observations were made from the microstructure examinations:

(a) Blended powder (A) produced non-uniform pores in the sample and excessive grain growth from longer sintering times.

TABLE 4

IDENTIFICATION OF SAMPLES

(All Samples were Sintered at 1500°C)

| Designation | Method of Preparation | Sintering Time | Sintered Hardness HV | Erosion Rate mg Loss/100 g SC | Average Grain Size (Micron) |
|---|---|---|---|---|---|
| A1 | SC | 16 | 1320 | 6.4 | 4.7 |
| A2 | CIP | 2 | 1103 | 7.5 | 3.0 |
| B1 | SC | 16 | 1314 | 7.0 | 4.4 |
| B2 | SC | 2 | 1158 | 8.2 | 3.4 |
| B3 | CIP | 2 | 1124 | 7.2 | 3.4 |
| C1 | SC | 16 | 1657 | 5.5 | 6.2 |
| C2 | CIP | 2 | 1627 | 4.9 | 4.2 |
| D1 | SC | 16 | 17.41 | 3.8 | 3.9 |
| D2 | CIP | 2 | 1309 | 8.8 | 2.0 |
| E1 | SC | 2 | 1815 | 4.4 | 1.8 |
| E2 | CIP | 2 | 1634 | 4.2 | 3.0 |

## PHOTOMICROGRAPHS OF SINTERED SAMPLES

| | | | |
|---|---|---|---|
| **Type:** | P - pressed; S - slipcast | **Sintering Temp:** | °C |
| **Material:** | % $Al_2O_3$ + % $ZrO_2$ | **Sintering Time:** | hours |
| **Sample:** | | **Avg. Grain Size:** | microns |

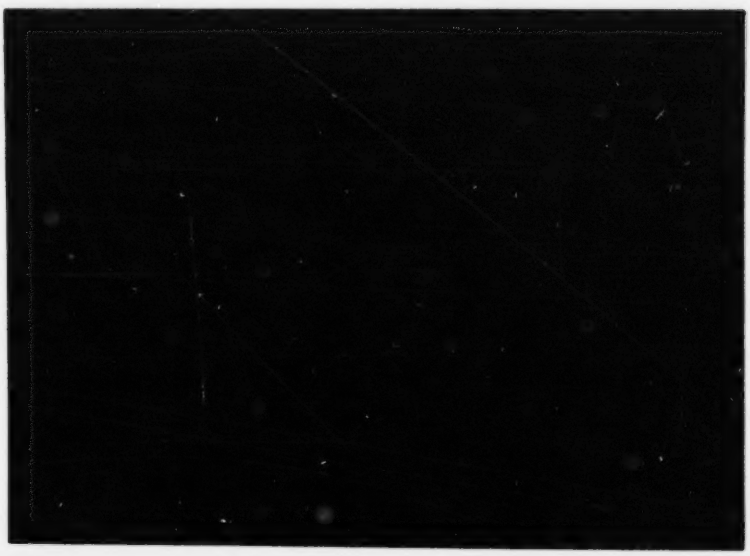

S
(N50+R50)+C
A1

1500
16
4.7

X1300

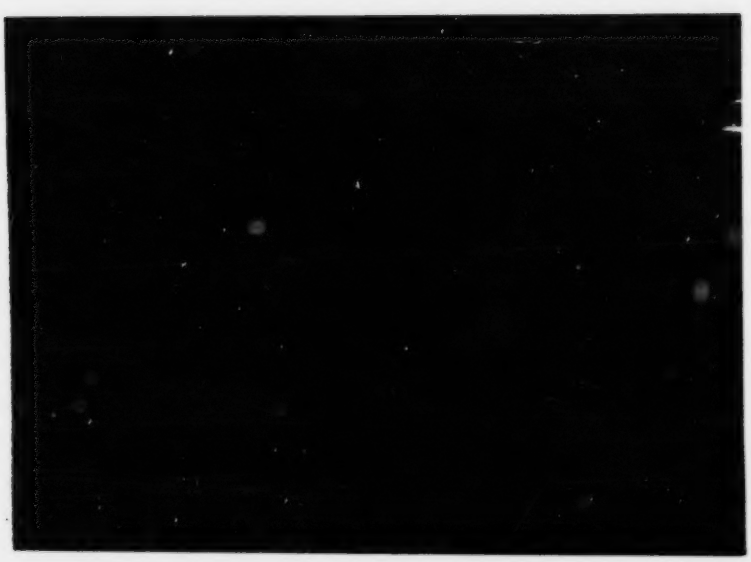

P
(N50+R50)+C
A2

1500
2
3

X1300

Figure 1

## PHOTOMICROGRAPHS OF SINTERED SAMPLES

| | | | |
|---|---|---|---|
| **Type:** | P - pressed; S - slipcast | **Sintering Temp:** | °C |
| **Material:** | % $Al_2O_3$ + % $ZrO_2$ | **Sintering Time:** | hours |
| **Sample:** | | **Avg. Grain Size:** | microns |

S
(R-47.5+N-47.5)
B1

1500
16
4.4 μ

X1300

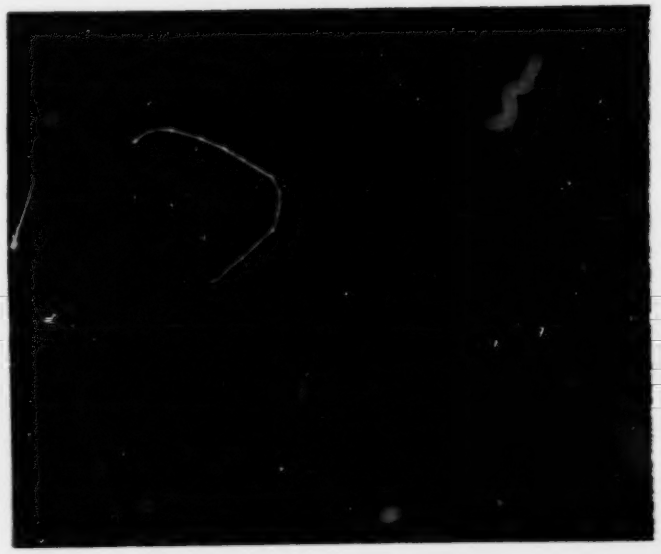

S
(R-47.5+N-47.5)+5
B2

1500
2
3.4 μ

Figure 2

X1300

## PHOTOMICROGRAPHS OF SINTERED SAMPLES

| | | | |
|---|---|---|---|
| **Type:** | P - pressed; S - slipcast | **Sintering Temp:** | °C |
| **Material:** | % $Al_2O_3$ + % $ZrO_2$ | **Sintering Time:** | hours |
| **Sample:** | | **Avg. Grain Size:** | microns |

P 1500
(R-47.5+N-47.5)+5 2
B3 3.4

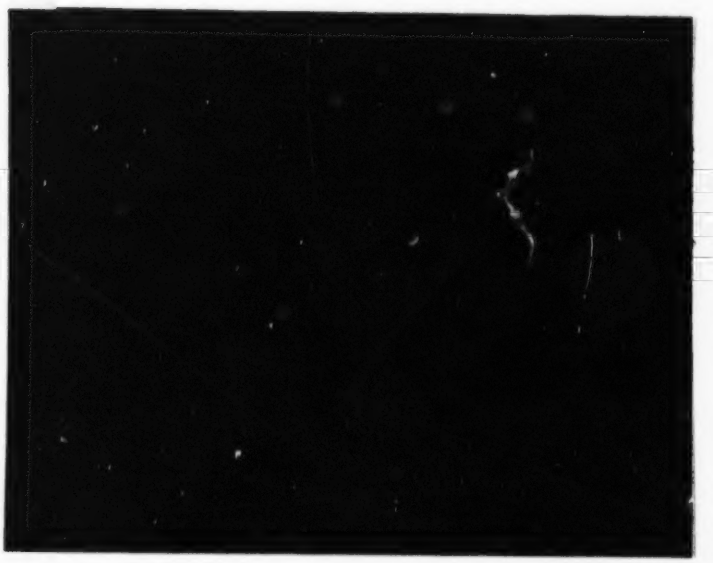

X1300

Figure 3

## PHOTOMICROGRAPHS OF SINTERED SAMPLES

| | | | |
|---|---|---|---|
| **Type:** | P - pressed; S - slipcast | **Sintering Temp:** | °C |
| **Material:** | % $Al_2O_3$ + % $ZrO_2$ | **Sintering Time:** | hours |
| **Sample:** | | **Avg. Grain Size:** | microns |

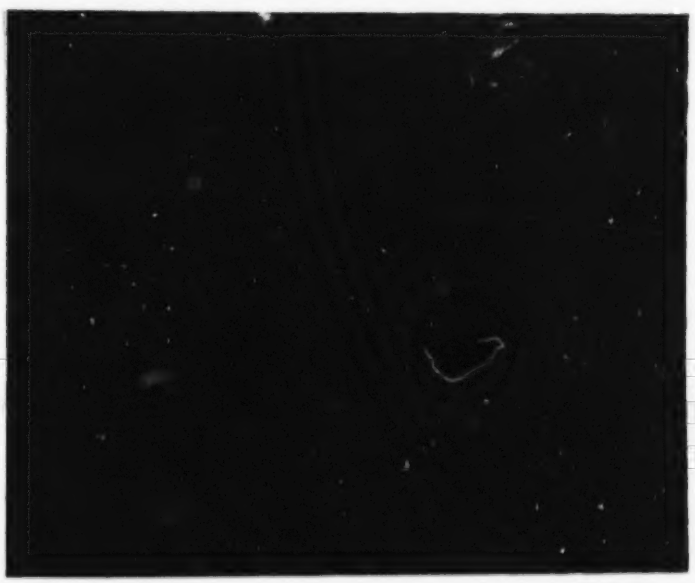

S
(A-39-100+0)
C1

1500
16
6.2 μ

X1300

P
(A-39-100+0)
C2

1500
2
4.2 μ

X1300

Figure 4

## PHOTOMICROGRAPHS OF SINTERED SAMPLES

| | | | |
|---|---|---|---|
| **Type:** | P - pressed; S - slipcast | **Sintering Temp:** | °C |
| **Material:** | % $Al_2O_3$ + % $ZrO_2$ | **Sintering Time:** | hours |
| **Sample:** | | **Avg. Grain Size:** | microns |

S
(%Alcoa 39-95)+5
D1

1500
16
3.9 μ

X1300

P
(%Alcoa 39-95)+5
D2

1500
2
2 μ

Figure 5

X1300

## PHOTOMICROGRAPHS OF SINTERED SAMPLES

| | | | |
|---|---|---|---|
| **Type:** | P - pressed; S - slipcast | **Sintering Temp:** | °C |
| **Material:** | % $Al_2O_3$ + % $ZrO_2$ | **Sintering Time:** | hours |
| **Sample:** | | **Avg. Grain Size:** | microns |

S
(A16-95)+5
E1

1500
2
1.8 μ

X1300

P
(A16-95)+5
E2

1500
2
3 μ

Figure 6

X1300

(b) The grain growth in sample C1 (A-39 powder) was non-uniform and excessive. This powder did not have the grain refiner MgO like RC-HB-DBM.

(c) $ZrO_2$ acts as a grain refiner as was observed in Figure 5 for sample D1 sintered for 16 hours and sample D2 sintered for 2 hours.

(d) The sintered ceramics produced from both the A-39 and A16 powder with 5% $ZrO_2$ had fine grains ($\sim$ 2U) and were dense.

## 3.3 Hardness Measurements

The hardness of all samples tested in Table 2 was measured by a Vicker Hardness Tester. The results are given in Table 4. It was observed that dense ceramics examined in this study with smaller grains had higher hardness values.

## 3.4 Determination of Erosion Resistance

### 3.4.a Procedure

Samples were eroded in a modified gas-solids sand-blaster[14]. The erodent used was 80 grit silicon carbide supplied by General Abrasives Ltd. A sieve analysis indicated a narrow particle size distribution with an arithmetric, geometric and Sauter mean diameter of 207, 206 and 210 microns respectively. A schematic diagram of the erosion testing apparatus is shown in Fig. 7. The sample, usually 1.9 cm in diameter and 1.9 cm in height, was mounted on a movable sample holder. A flat surface of the sample was located 0.5 cm from the nozzle of a Metfor M-4 sand-blaster. The original collimating tube was replaced by an alumina tube to

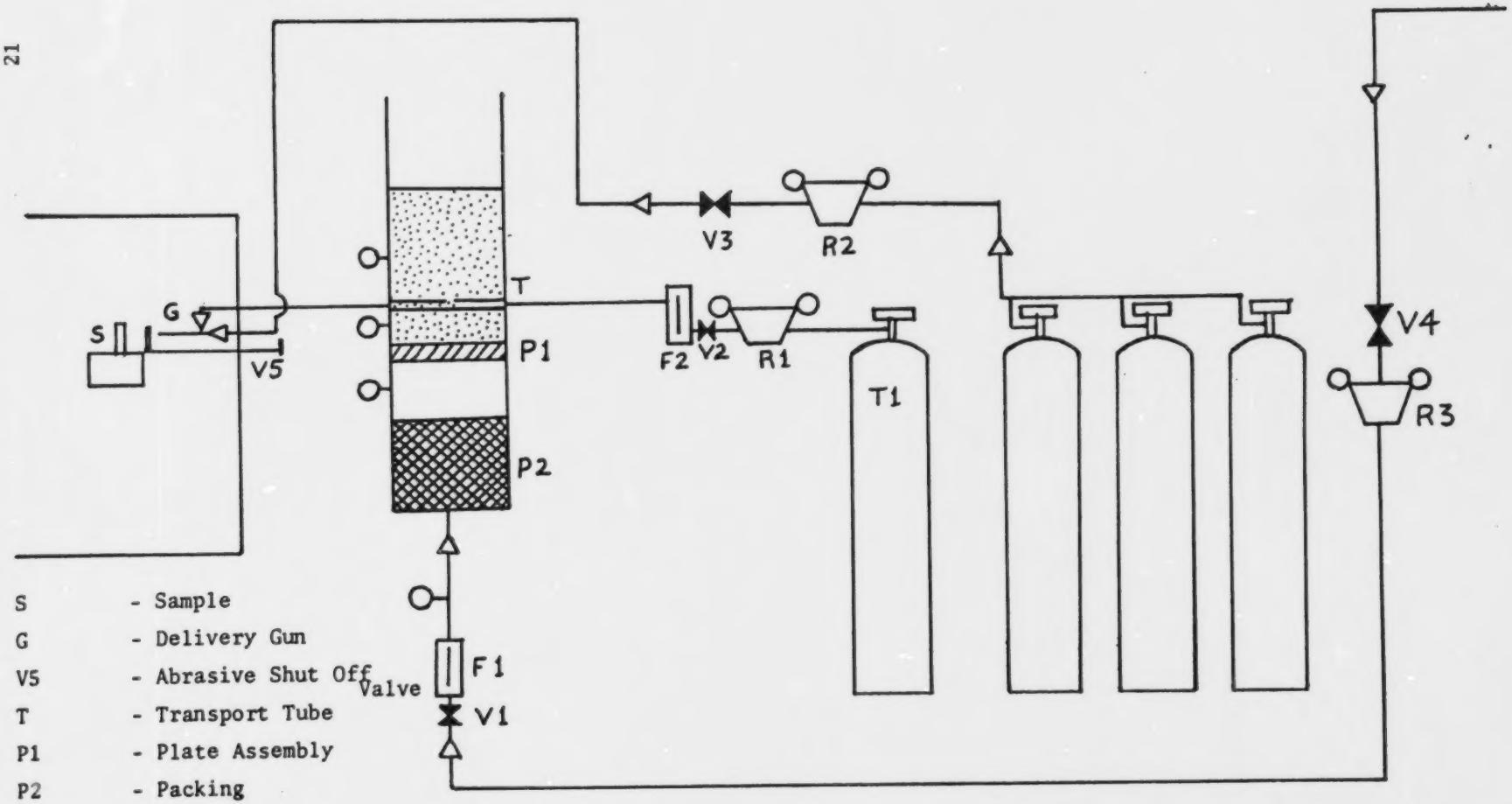


S - Sample
G - Delivery Gun
V5 - Abrasive Shut Off Valve
T - Transport Tube
P1 - Plate Assembly
P2 - Packing
F - Flow Meter
R - Air Regulator
V1 to V4 - Air Valves

Fig.7- SCHEMATIC OF ABRASIVE TEST APPARATUS

increase its service life. The alumina tube was replaced every 8-10 minutes to maintain a constant flow rate. The erodents were fed to the sand-blaster through Tygon tubing from a fluid bed feeder. In the fluidized bed of SiC particles was a horizontal feed tube with a small hole in its upper surface. Transport air blown through this feeder tube entrained SiC from the bed and fed it to the sand-blaster. With close control on the air flows the erodent flow rate could be maintained at about 5 $g.sec^{-1}$. The velocity of the particles was measured by the technique described by Ruff and was maintained at 32.5 $m.sec^{-1}$ at the nozzle.

A shield was placed in front of the sample while the flow of erodent was adjusted, whereupon the shield was removed and the sample eroded for 60 sec. Erosion of the sample was determined by weighing the sample before and after the test.

### 3.4.b Erosion Test Results

Erosion tests were performed on samples from powders A, B, C, D and E sintered at 1500°C. The results are shown in Table 4. For this work the erodent impinged on the sample at an angle of 90°; the rate of erosion is given in mg weight loss per 100 g of SiC used.

It was observed that the erosion rate was dependent mainly on the density of the sintered samples. There was also some indication that fine-grained dense ceramics had higher erosion resistance.

## 3.5 Thermal Shock Measurements & Results

### 3.5.a Procedure

The thermal shock test consisted of rapidly heating a sample to temperatures up to 1150 C by induction heating of an enclosing

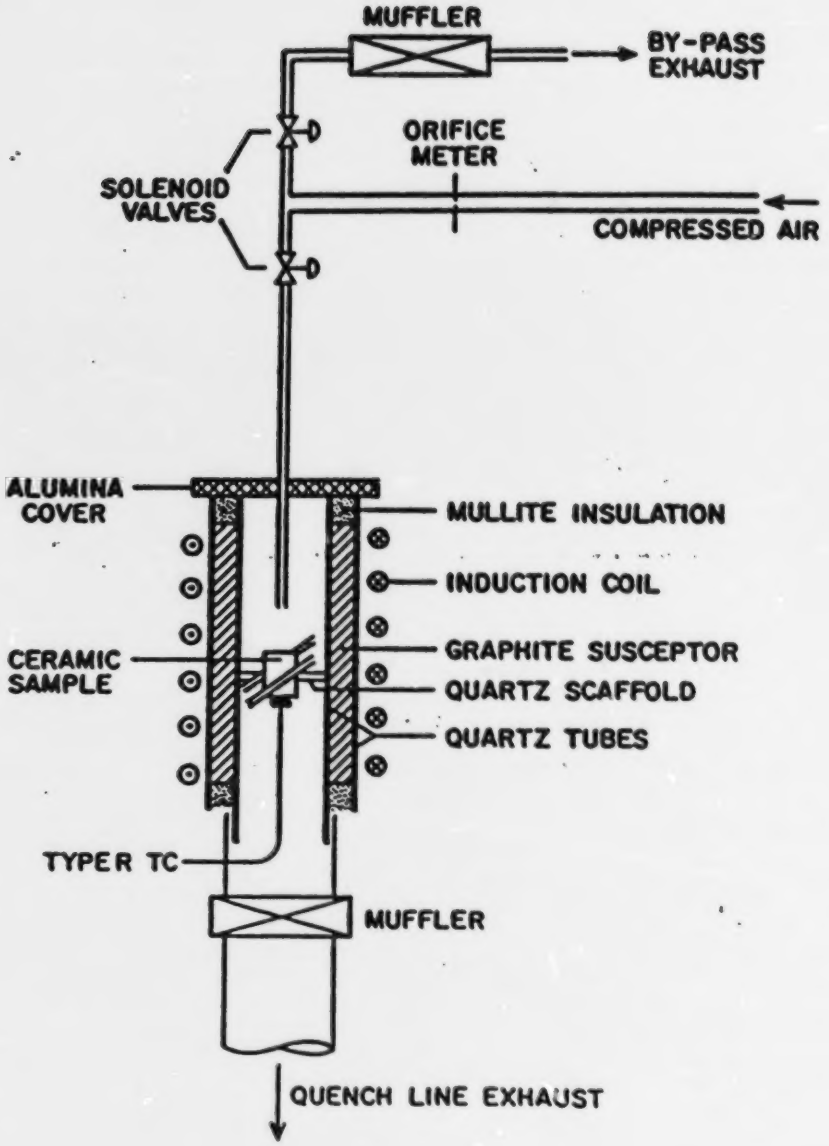


Figure 8 Schematic Diagram of Thermal Shock Test Apparatus

graphite sleeve, followed by rapid cooling by a blast of compressed air.

Figure 8 is a schematic diagram of the apparatus[14]. The cylindrical specimen sat on a scaffold constructed of three pairs of 0.2 cm diameter quartz rod fused to the side of a 3.15 cm i.d. quartz tube. The graphite susceptor surrounded the tube, and in turn was protected from air oxidation by an outside quartz tube. The induction coil was a 6 turn coil of 0.9 cm diameter copper tubing. The induction generator was a Lepel T-20 rated for 20 kW, maximum coil current of 400 amperes at a frequency of 400 kH. Positioned 2.5 cm above the sample was a quartz tube of 1.25 cm inside diameter which was used to direct compressed air onto the sample during the cooling part of a test cycle. Temperatures were monitored using a bare Type R thermocouple touching the bottom face of the test specimen.

The compressed air was delivered from a high capacity compressor, and its flow rate measured using an orifice plate. The Reynolds number in the blast tube could be made as high as 90,000.

To perform a thermal shock test, the specimen was heated at the maximum heating rate available up to a predetermined temperature (maximum 1150 C). During this time a preselected air flow was established and allowed to become constant while flowing to waste. When the required temperature of the test specimen had been achieved then simultaneously the power to the induction coil was shut off and the flow of quenching air diverted to the sample quenching line.

Cylindrical specimens 1.9 cm in diameter and 1.9 cm in length were heated at rates of about $3°C.sec^{-1}$ to a predetermined temperature (max. 1150°C). Then they were rapidly cooled, at rates of about $10°C.sec^{-1}$ by a blast of compressed air. After each heating-cooling cycle, the sample was examined visually for the presence

of cracks. If no cracks were detected upon careful examination the sample was subjected to more severe conditions until it failed. For each type of sample a failure-envelope becomes delineated in terms of the two variables: temperature and Reynolds number. A failure index was derived from this envelope.

Admittedly, in this ad. hoc. test the method of detecting the occurrence of cracks is subjective, and micro-cracks may go unnoticed. However, it is considered that the procedure is at least self-consistent, and serves adequately to compare thermal shock resistances. The method resembles in some respects that of Faber, Huang and Evans[16] in which a heated ceramic disc, 5 cm in diameter and 0.25 cm in thickness is shock-cooled by a blast of air (Reynolds number about 20,000) directed at its centre. The thin disc used by Faber et al. is more amenable to stress analysis than the cylinder used in this work.

### 3.5.b Thermal Shock Test Results

Figures 9 to 19 show data of temperatures and cooling rates for samples tested in Table 2. All data were plotted on graphs where the temperature axis was 500-1300°C and Reynolds number axis was 0-100000. The area to the left of the failure envelope then was calculated as a percentage of the total area, and used as the failure index. Index falls between 0-100 with a larger number inferring a better thermal shock resistance. The results are given in Table 5.

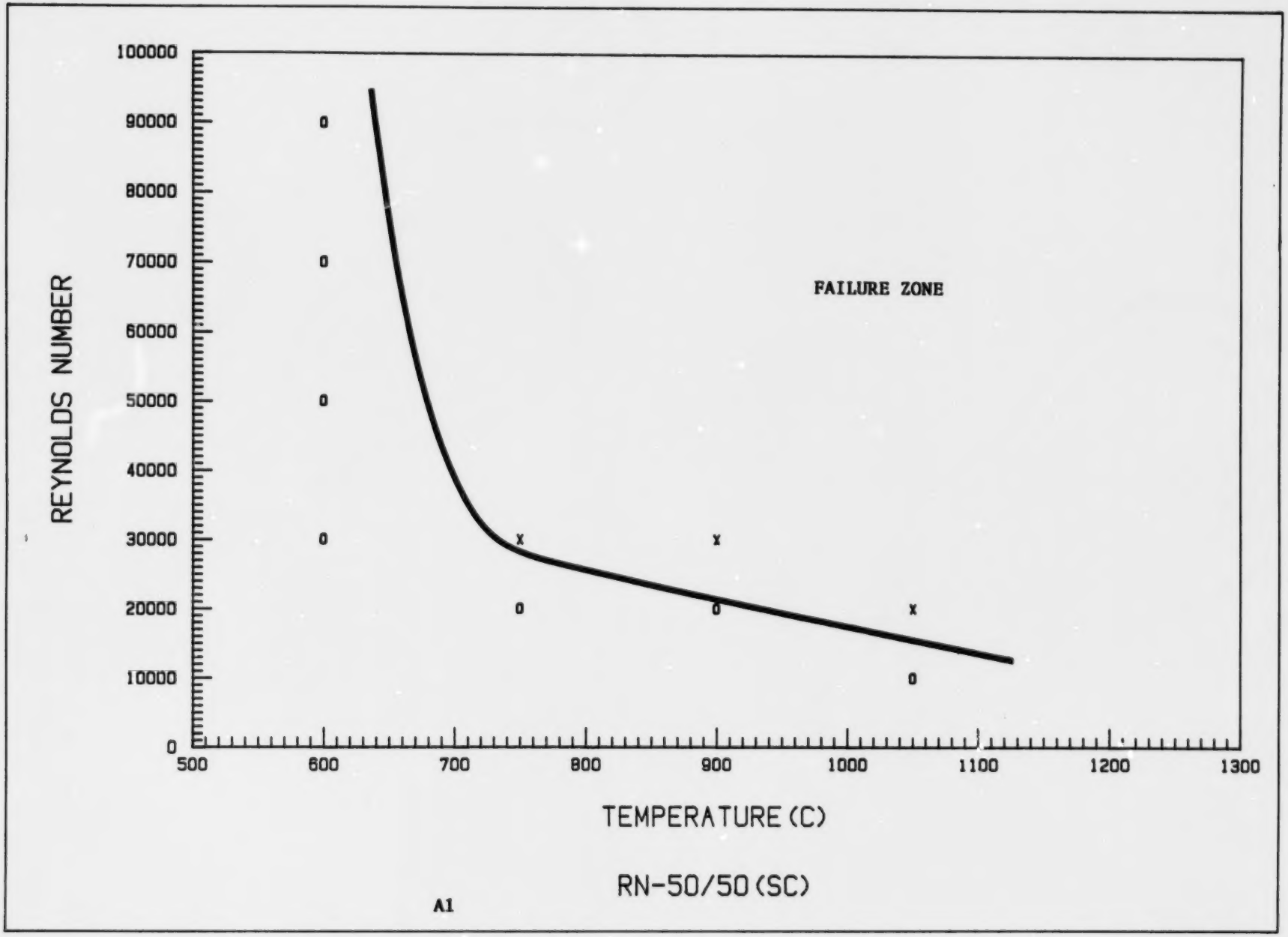


Figure 9 Failure Zone Plot of Sample A1

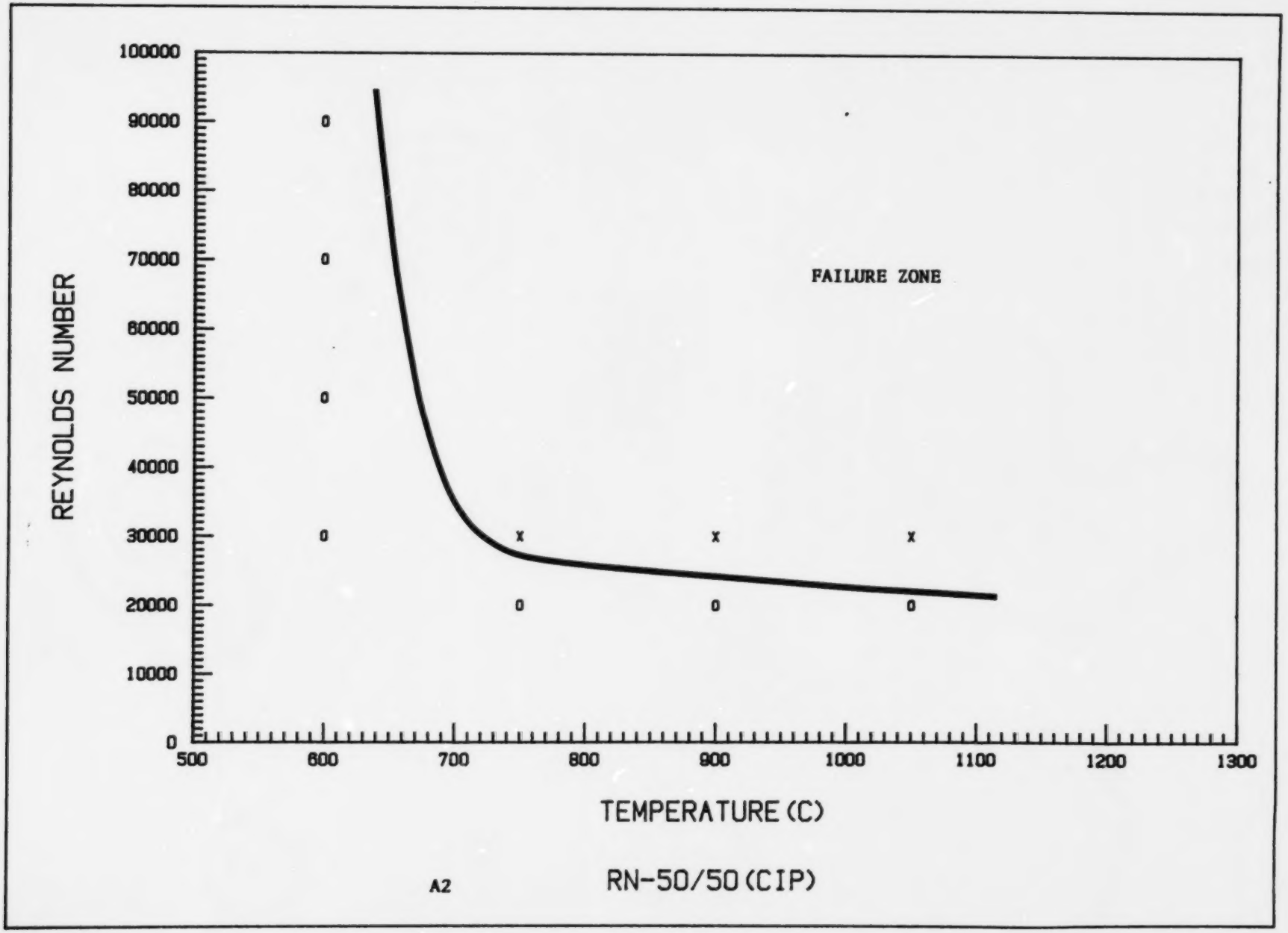


Figure 10 Failure Zone Plot of Sample A2

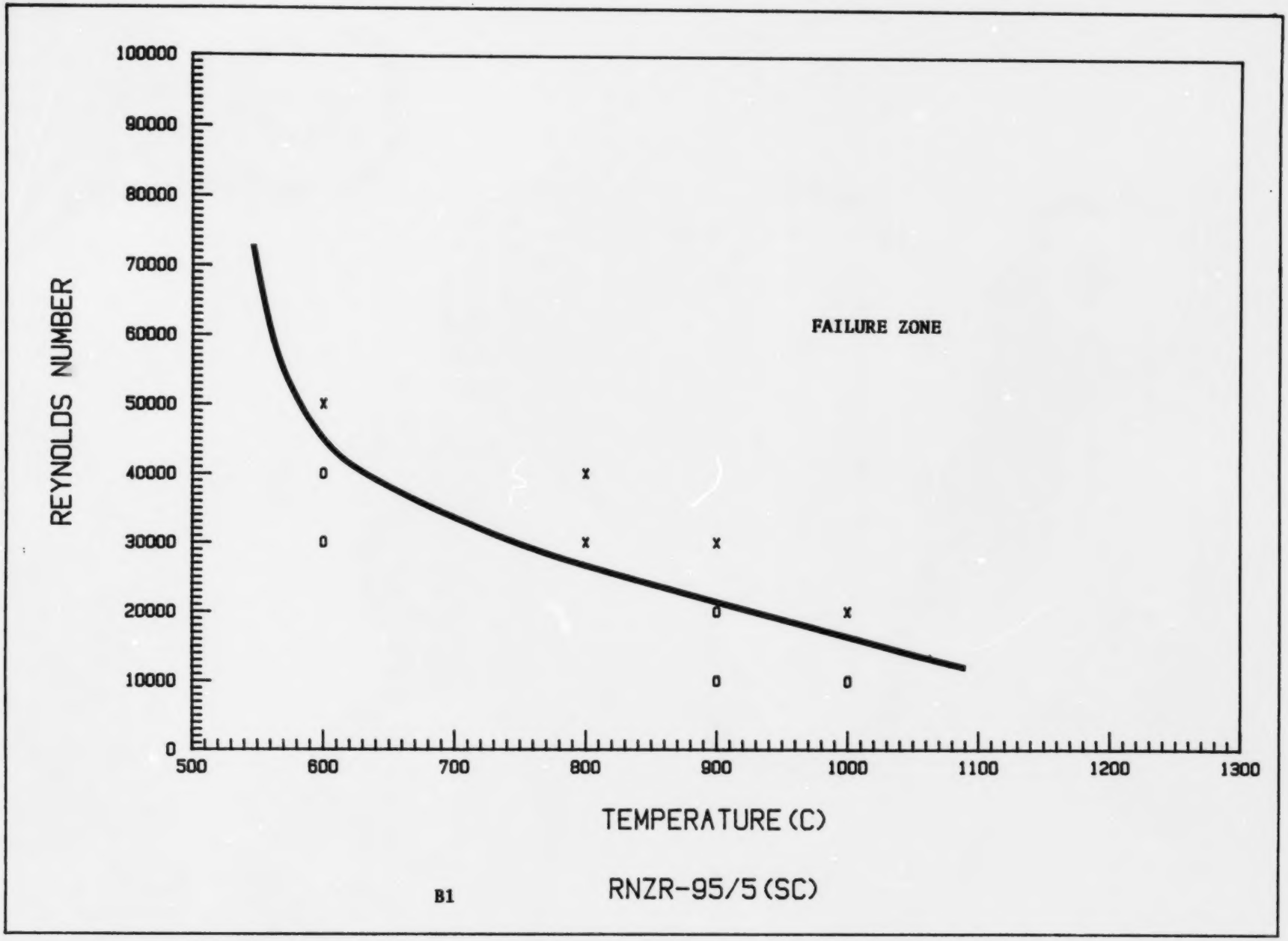


Figure 11 Failure Zone Plot of Sample B1

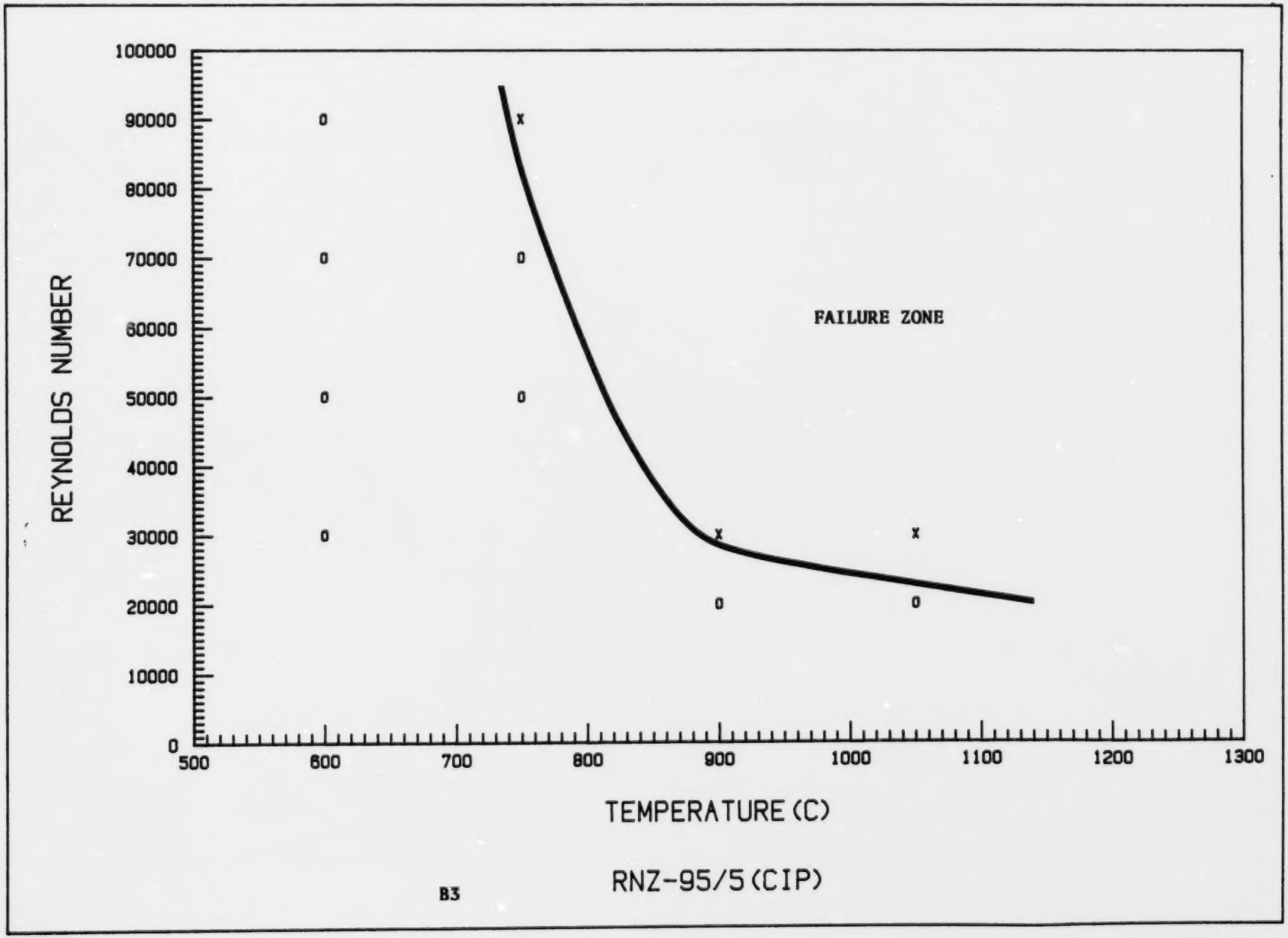


Figure 12 Failure Zone Plot of Sample B3

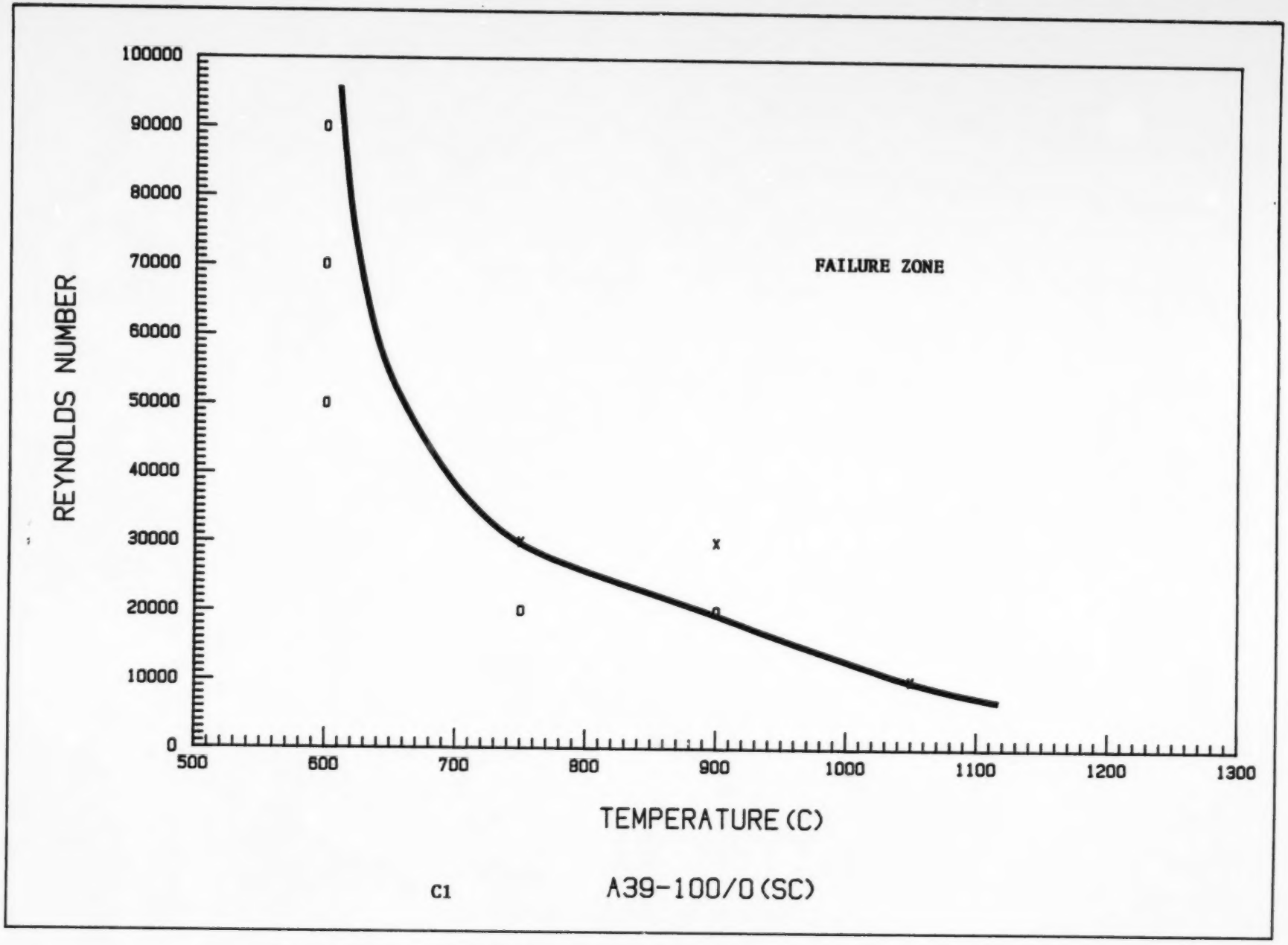


Figure 13 Failure Zone Plot of Sample C1

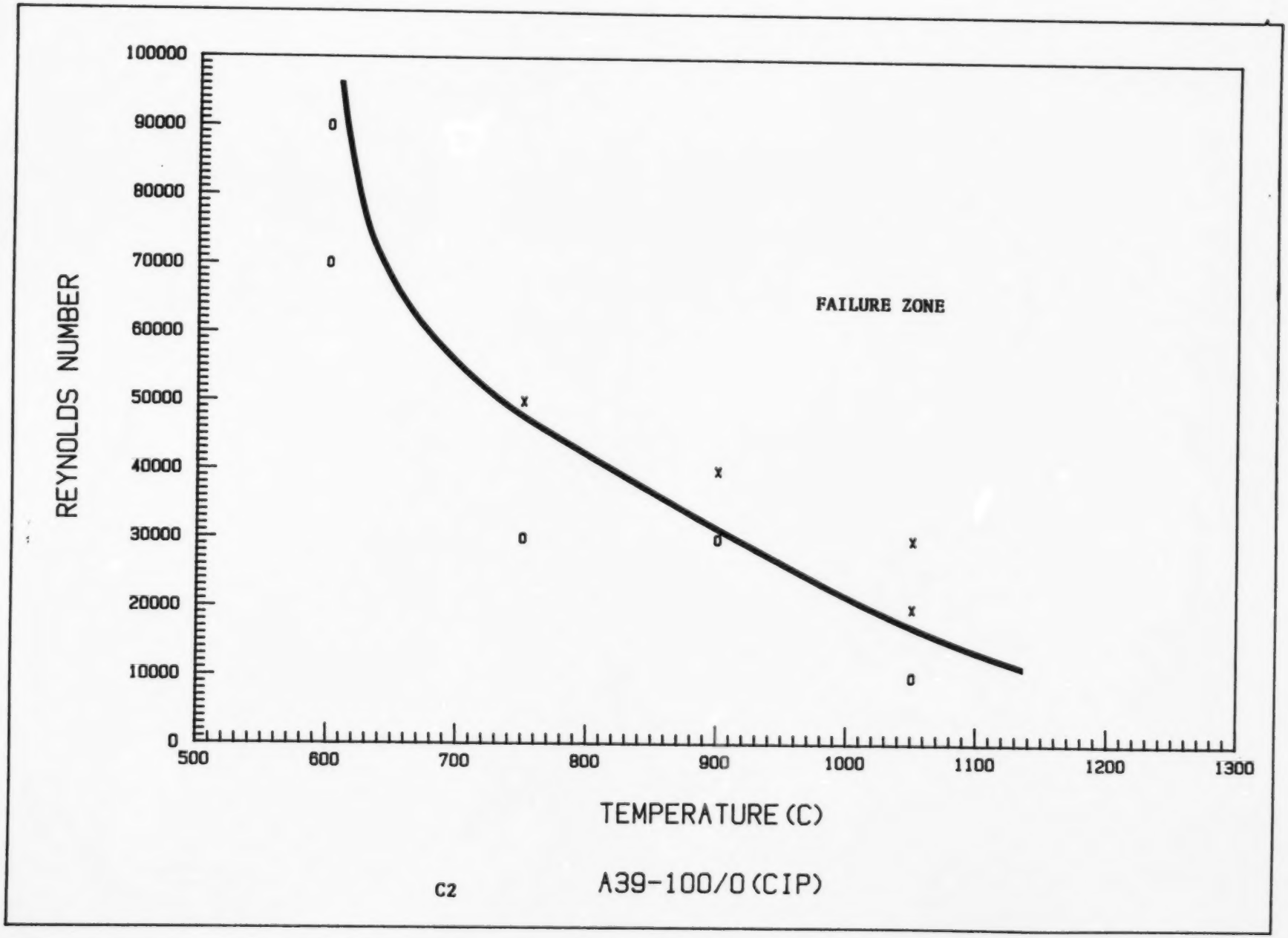


**Figure 14** **Failure Zone Plot of Sample C2**

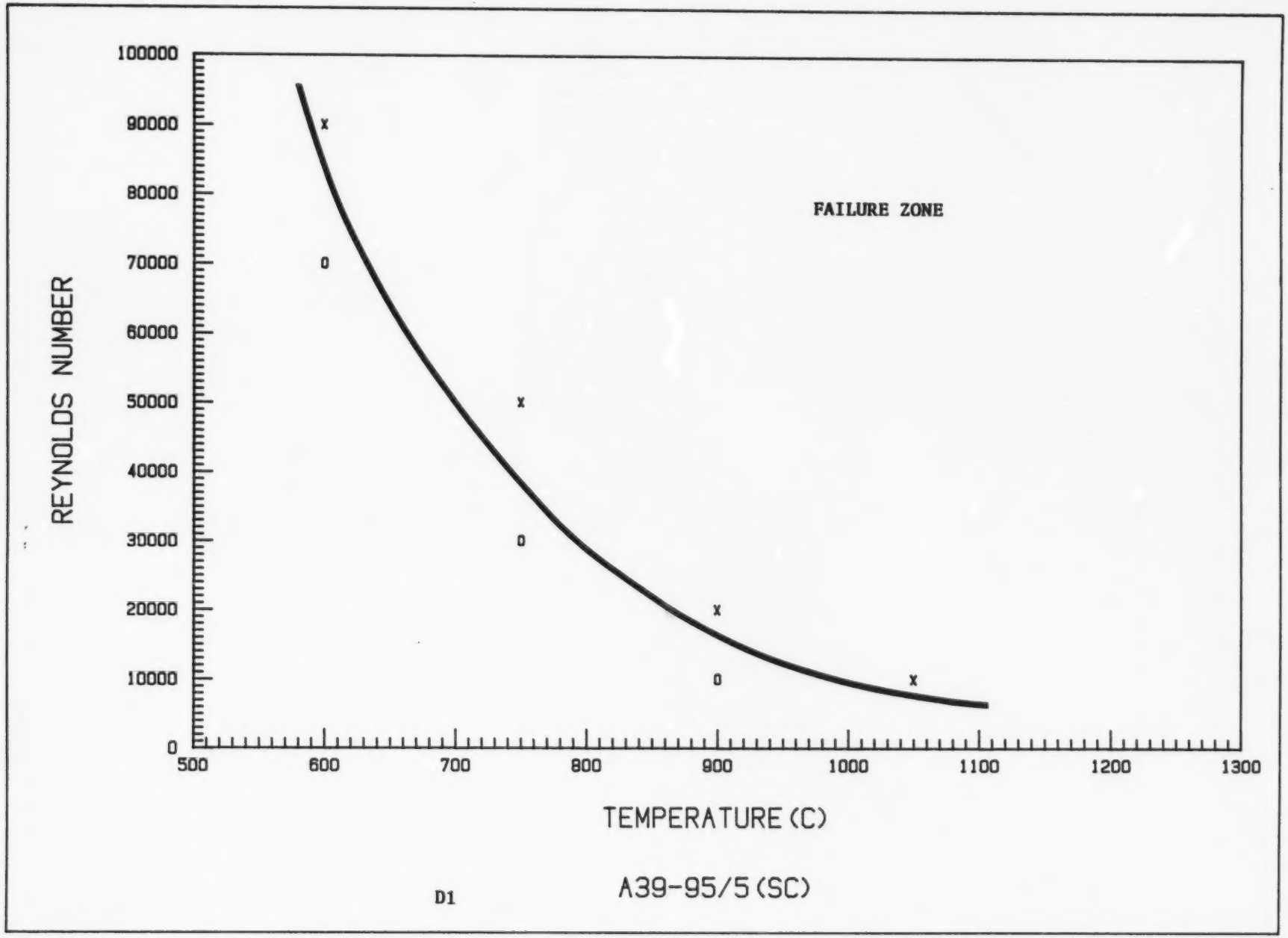


Figure 15 Failure Zone Plot of Sample D1

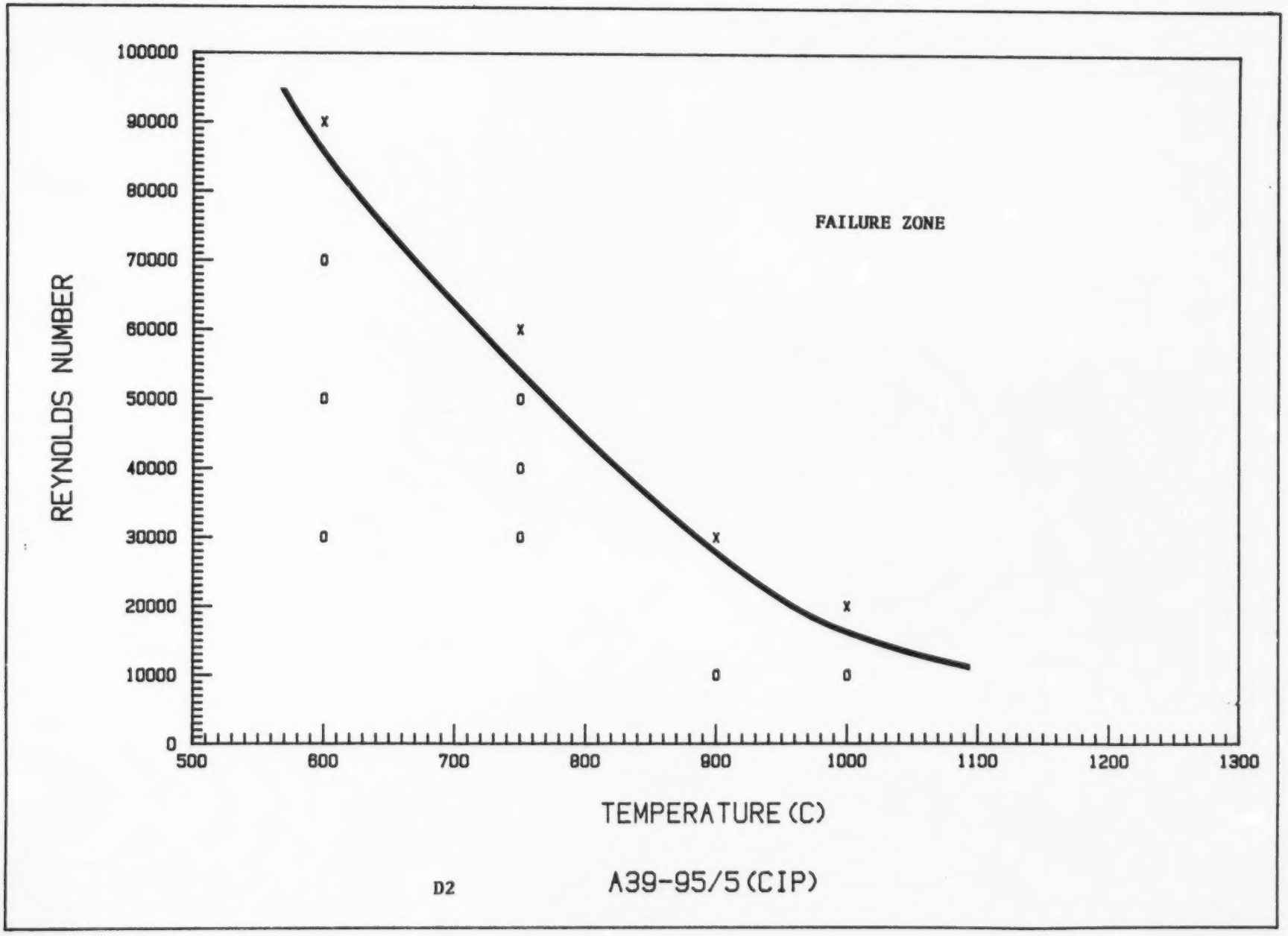


Figure 16 Failure Zone Plot of Sample D2

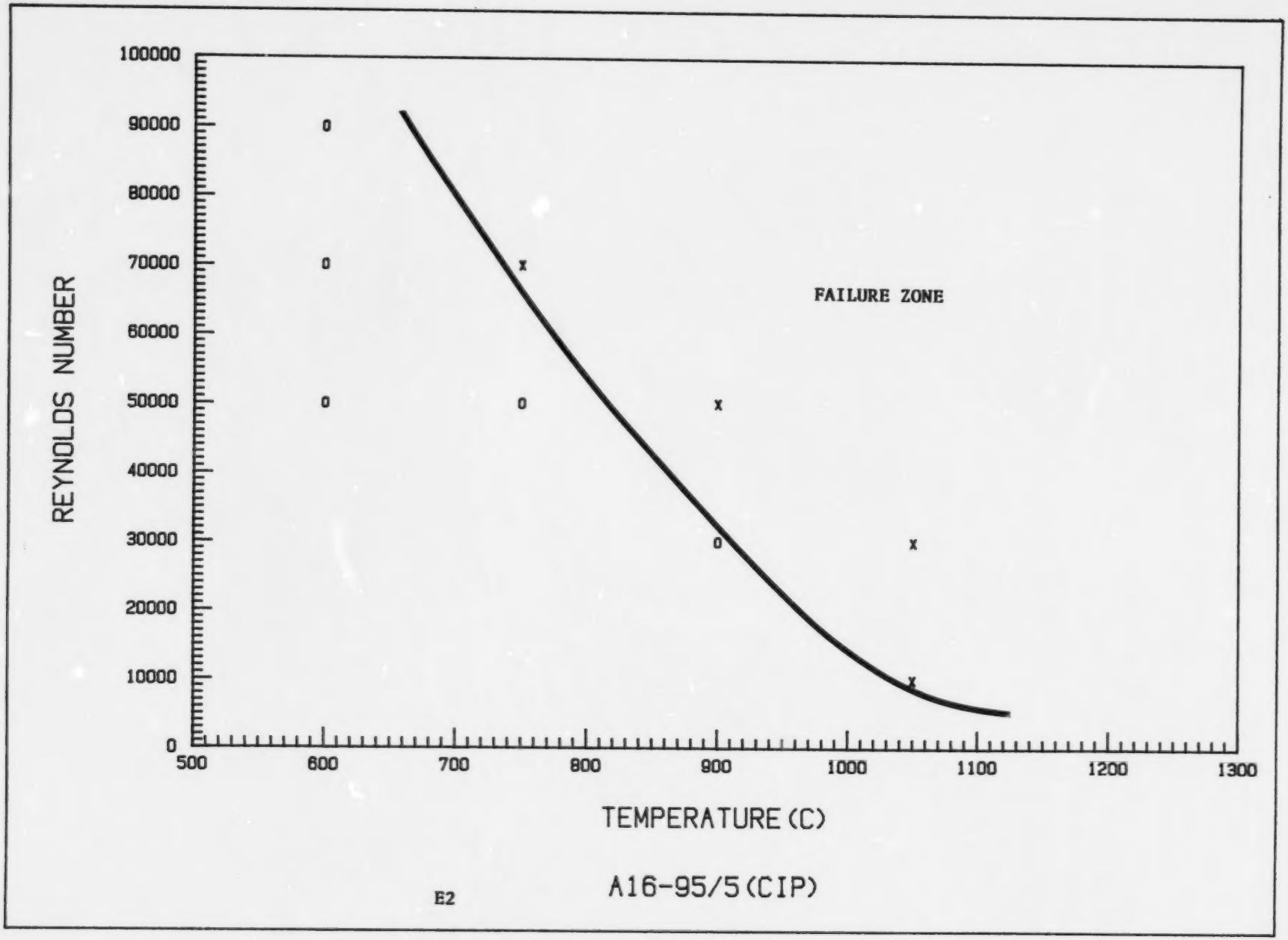


Figure 17 Failure Zone Plot of Sample E2

TABLE 5

FAILURE INDEX

| Sample | Specimen | Casting Method | Sintering Time Hrs. | Failure Index |
|---|---|---|---|---|
| A1 | 50% N + 50% RC-HB-DBM | SC | 16 | 36 |
| A2 | 50% N + 50% RC-HB-DBM | CIP | 2 | 40 |
| B1 | 95% A + 5% $ZrO_2$ | SC | 16 | 27 |
| B2 | 95% A + 5% $ZrO_2$ | SC | 2 | |
| B3 | 95% A + 5% $ZrO_2$ | CIP | 2 | 51 |
| C1 | 100%/0% - A39 | SC | 16 | 32 |
| C2 | 100%/0% - A39 | CIP | 2 | 41 |
| D1 | 95%/5% $ZrO_2$ - A39 | SC | 16 | 32 |
| D2 | 95%/5% $ZrO_2$ - A39 | CIP | 2 | 40 |
| E1 | 95%/5% $ZrO_2$ - A16 | SC | 2 | |
| E2 | 95%/5% $ZrO_2$ - A-16 | CIP | 2 | 43 |

SC = Slipcasting

CIP = Cold Isostatic Press

No failure at all conditions - 100.

The higher the index, the better the thermal shock resistance.

# SPECIMEN DIMENSIONS AND LOADING GEOMETRY FOR FRACTURE TOUGHNESS TEST

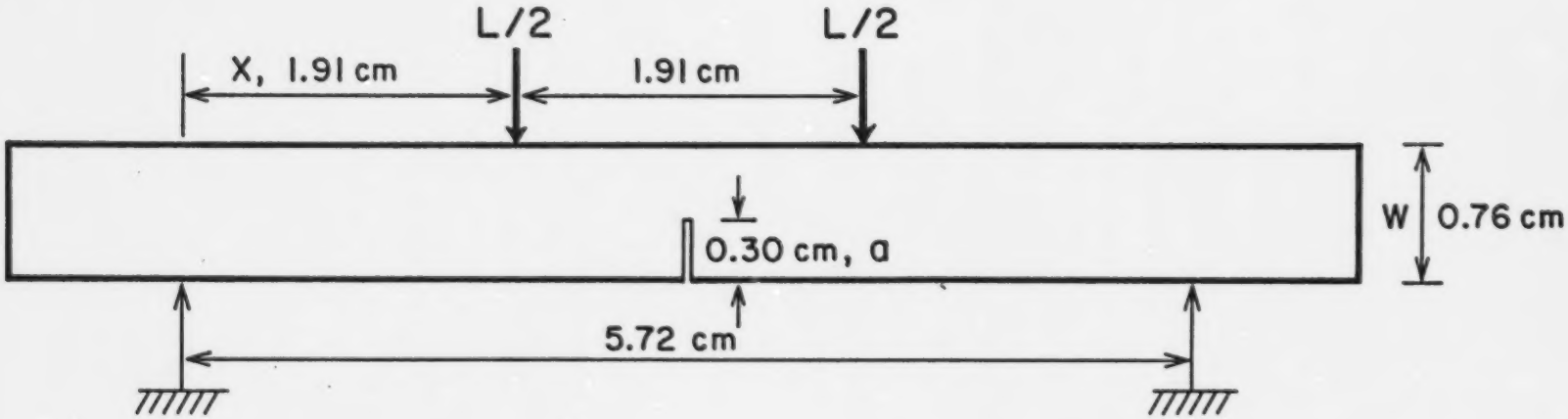


Thickness – 0.61 cm (b)
Width of slot – 0.020 cm

Figure 18 Single Edge Notched Bend Specimen

## 3.6 Fracture Toughness Measurements

### 3.6.a Procedure

A significant number of techniques for determining the crack growth resistance of brittle materials are available. The single edge notch bend specimen (SENB) was used for fracture toughness measurements. The SENB technique was used because of its simplicity and the ease of specimen preparation.

Specimens were produced by slipcasting, presintering and subsequently grinding them down to size with a surface grinder. The notch was cut with an alumina abrasive wheel. The expected final dimensions of samples calculated on the basis of 16% shrinkage are shown in Figure 18.

The dimensions chosen were of the same ratios used by Munz et al.[17]. The fracture toughness of specimens was tested by a four-point bend test jig. Four-point loading was preferred over three-point bending because of the constant bending moment between the inner loading points, thus specimen alignment was not critical. In addition, interaction between the load roller stress field and the crack stress field, which can happen in three point bending, was avoided.

The test jig was designed and built here at NSRFC. The jig is shown in Figure 19.

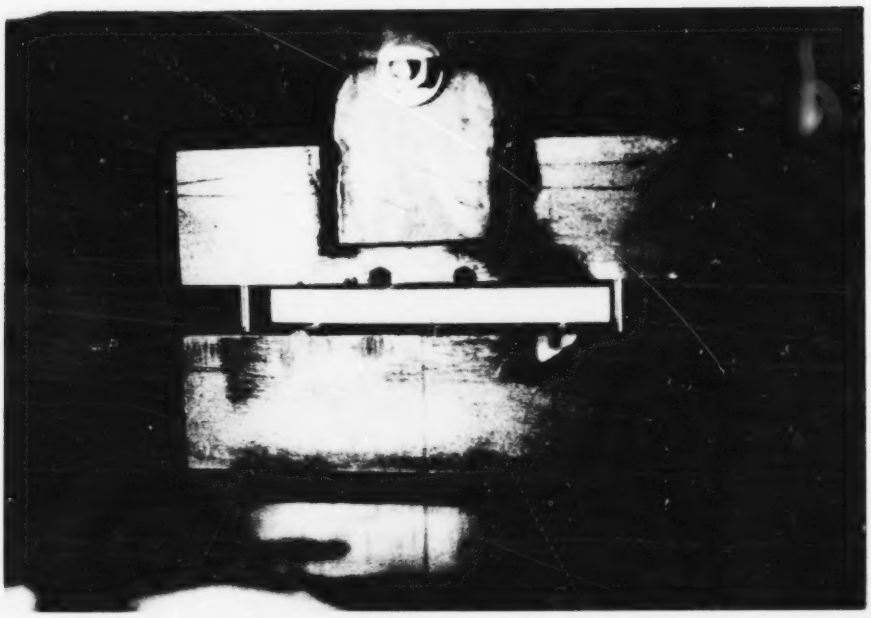

**Figure 19** **Testing of a Fracture Toughness Specimen**

Testing was performed on a model 810MTS materials testing system. The actuator speed was 0.05 mm/min. Load was recorded as a function of actuator displacement. $K1_C$ was evaluated using the Griffith relation:

$$K1_C = \frac{6Ma^{\frac{1}{2}}}{bw^2} \cdot Y \qquad (1)$$

Where:

Y = dimensionless parameter = $1.99-2.47(a/w)+12.97(a/w)^2-23.17(a/w)^3+24.80(a/w)^4$ for 4 point bending

M = applied bending moment = P/2(X)

a = crack length

b = width

w = thickness

The Griffith relation simplifies to equation 1 for the specimens used in this particular test.

$$K1_C = \frac{9/4\ P\ a^{\frac{1}{2}}}{b.w^2}.\ Y \qquad (2)$$

### 3.6.b Fracture Toughness Results

The results are given in Table 6. The values are average of 6 to 12 individual results. The test data are given in Appendix B. The results varied from 4·45 to 5·9 MPa$\sqrt{m}$. The ceramic sample (E1) produced from A-16 + 5% $ZrO_2$ powder had the maximum toughness.

TABLE 6

FRACTURE TOUGHNESS RESULTS

| Sample | $K1_C$(MPa $\sqrt{m}$) |
|---|---|
| A1 | 4.84 (average of 8) |
| B1 | 5.08 (average of 6) |
| C1 | 4.45 (average of 12) |
| D1 | 4.65 (average of 9) |
| E1 | 5.90 (average of 7) |

## 4. DISCUSSION

A linear regression analysis was performed on hardness Vs % theoretical density, hardness Vs erosion rate and % theoretical Vs erosion rate. The plotted results are given in Figures 20, 21 and 22. The best fit linear equations with standard deviations are also presented with the figures.

In general, the erosion rates appear to be directly related to both the hardness and % theoretical densities. For instance, samples A2, B2, and B3 with lower % theoretical densities and hardnesses had higher erosion rates; whereas samples C1, C2, D1, E1 and E2 with higher % theoretical densities had higher hardness and higher erosion resistance. The reason for the % theoretical density of sample D2 being higher than expected, considering its hardness and erosion rate, cannot be explained and is suspected to be the result of experimental error.

The influence of sintered grain size and the addition of $ZrO_2$ in the composite on the properties of these ceramics was also investigated. Non-uniform grain growths decreased the erosion resistance as was observed in sample C1. Sample C1 (% theoretical density of $\sim$ 98 and hardness $\sim$ 1600) produced from A-39 powder had a higher erosion rate (5.5 mg/100 SiC) than that of C2 specimen (4.9 mg/100 SiC) having similar hardness and density. Erosion mechanism through intergranular brittle fracture satisfies the above findings. The influence of $ZrO_2$ addition to $Al_2O_3$ powder was found to be two fold. $ZrO_2$ retards grain growth, thereby erosion rate and improves toughness. The grain size and erosion rate of sample C1 (A-39 pure $Al_2O_3$) was greater than sample D1 (A-39 + 5% $ZrO_2$), a composite.

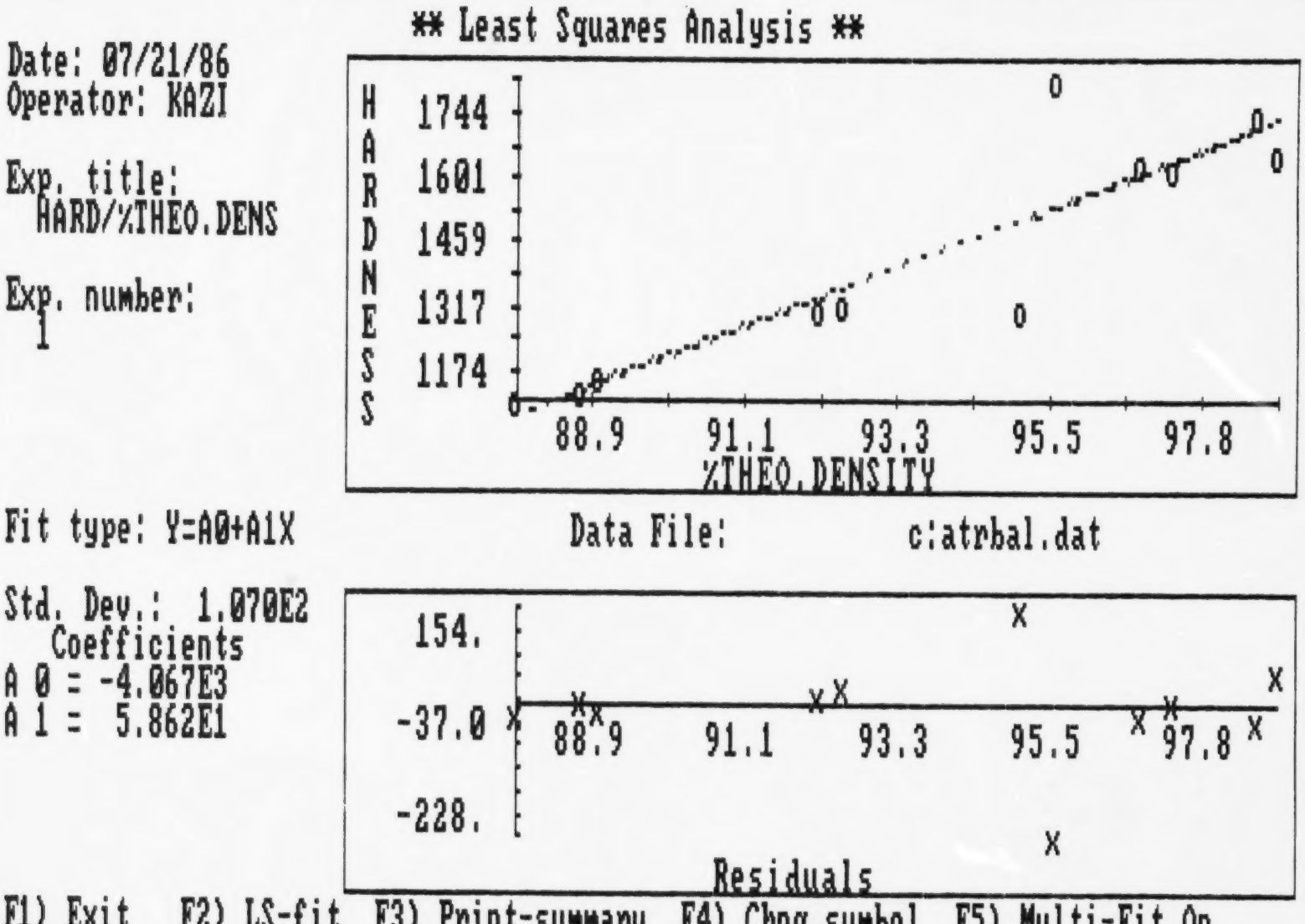


Figure 20 Hardness Vs % Theoretical Density

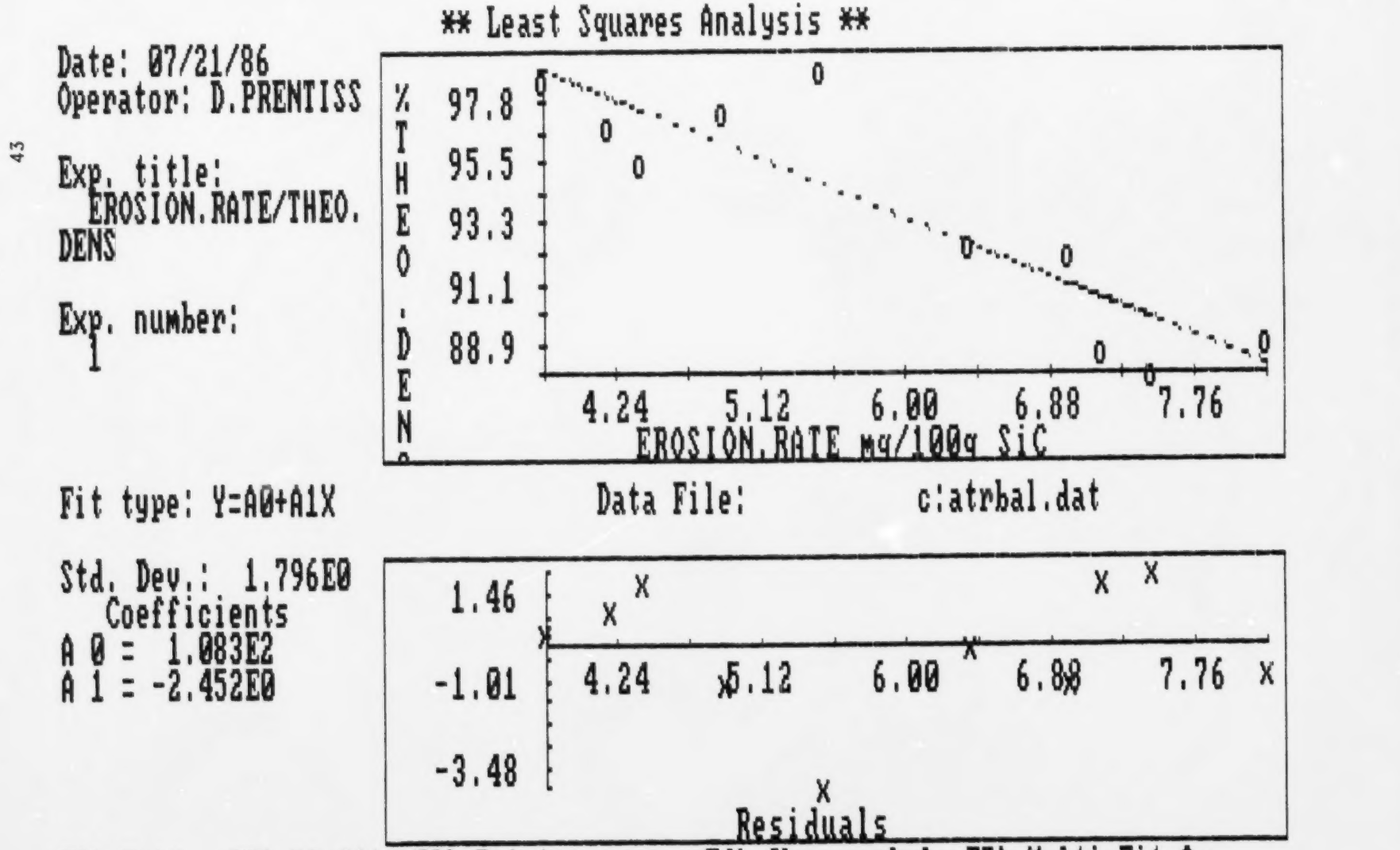


Figure 21 % Theoretical Density Vs Erosion Rate

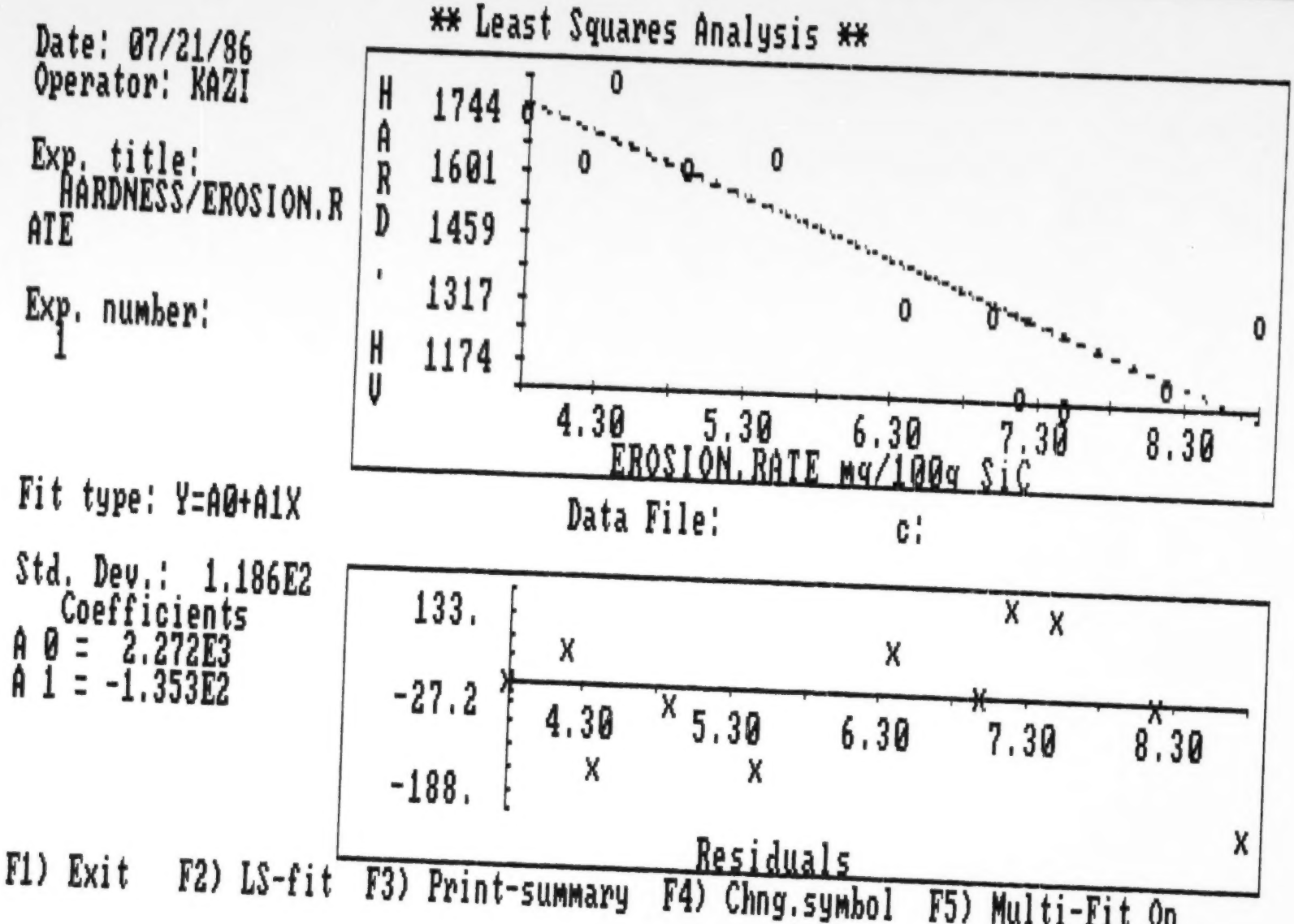


Figure 22

Hardness Vs Erosion Rate

The decrease of erosion rate due to the presence of $ZrO_2$ was also reported by J.H. Giovanola (18). Fracture toughness values are given in Table 6. Fracture toughness was improved by the addition of 5 Wt% $ZrO_2$ in all three types of powder studied. The most pronounced effect was found with Alcoa-16 (A-16) powder. A study conducted by Becher and Tennery(1) used a four-point bend method similar to the one in this work, and formed the composites through sol-gel route. They found that the fracture strength of their alumina was about 4 MPa$\sqrt{m}$, increased to 6.5 for a 10 Vol % addition of $ZrO_2$. Our results are in agreement with these. The fracture toughness of specimens prepared from Alcoa-16 (A-16) + 5 Wt.% $ZrO_2$ was 5.90 (average of 7) MPa$\sqrt{m}$.

The thermal shock resistance of a few porous samples was better than dense ceramics. Figure 12 presents the thermal shock data for porous sample B3. There existed a base-line temperature ($\sim$ 800°C) below which failure was not detected visually even at a highest attainable Reynolds number (90,000) of the cooling air. One the other hand, there were some high temperatures above which failure occurred even at the lowest flow rate used, Re = 20,000. Between these two temperatures, failure would depend upon the severity of the quench. In comparison, the base-line temperature for C1 (Figure 13) sample is 600°C and the Re is 12,000 for the lowest flow rate at higher temperature. Not all dense ceramics studied in this project followed the above relationship as was also reported in the previous communication(14). Compared to the ceramics examined in this study the thermal shock resistance of E1 (A-16 material) sample was quite good.

Of all samples examined, E1 and E2 produced from 95 Wt% $Al_2O_3$ (A-16) + 5 Wt% $ZrO_2$ had the finest grain sizes ($\sim$ 2 U). The distribution of the second phase $ZrO_2$ appears to be fairly uniform. Longer sintering times (16 hours) resulted in grain growths for both pure $Al_2O_3$ (C1) and $Al_2O_3$ + $ZrO_2$ composite (D1). Excessive and

non-uniform growth occurred only in pure $Al_2O_3$ (C1).

The sintered density of C1 (A-39 powder) and D1 (A-39 + 5% $ZrO_2$) samples was 98% of the theoretical value; whereas the % theoretical density of E2 (A-16 + 5% $ZrO_2$) sample was lower (about 97%). No attempts were made to optimize the density of these ceramics by adjusting the sintering temperature or time. A sintering temperature of 1500°C and a soaking time of 2 hours are considered adequate to obtain nearly full density for fine alumina powders without grain enlargement. Considering the porosity (3%-4%) of E1 and E2 samples, the hardness and erosion resistance were good compared to fine-grained dense $Al_2O_3$ ceramics previously reported[19].

The sintered density of samples prepared from 50% by weight of 12 day ball-milled Norton powder (median size 0.92 U) blended with 50% by weight of RC-HB-DBM powder (median size 0.55 U), was less than the density of sintered ceramics produced from 100% Norton powder or 100% RC-HB-DBM powder. It appears that the density of sintered ceramics depends critically on the grain size distribution of powder used.

## 5. CONCLUSIONS

The erosion rate was dependent mainly on the density of the sintered specimens, while independent of the type of alumina or alumina composite used.

The range of densities observed was due to the combination of the different powders, different sintering times, and use of both slipcasting and isostatic pressing.

Slipcast samples in general had smaller shrinkages than that of pressed samples. It was easier to prepare slurry of proper consistency to obtain solid casts for Alcoa-16 power or composites of Alcoa-16 with $Zr0_2$ than Alcoa-39 powder.

Ceramics produced from Alcoa-16 + 5 wt% $Zr0_2$ had better erosion resistance, finer grains, relatively higher hardness and comparable thermal shock resistance to all other ceramics studied in this project.

The $K1_c$ value of Alcoa-16 + 5 wt% $Zr0_2$ composite (A-16; \$<1/lb; purity 99.70, median size 0.55U) was greater than the composite prepared from Alcoa-39 (A-39; \$12/lb; purity 99.90, median size 0.50U) + 5 wt% $Zr0_2$ and the specimens prepared for RC-HB-DBM + 5% $Zr0_2$ (RC-HB-DBM; \$14/lb; purity 99.95, median size 0.55) as reported in a previous work[19]. $K1_c$ values are listed below:

| Material | Treatment | $K1_c$ $MPa\sqrt{m}$ |
|---|---|---|
| Alcoa-16 + 5% $Zr0_2$ | Sintered 1500°C,2hrs. | 5.90 |
| Alcoa-39 | Sintered 1500°C,2hrs. | 4.45 |
| Alcoa-39 + 5% $Zr0_2$ | Sintered 1500°C,2hrs. | 4.65 |
| RC-HB-DBM* | Sintered 1500°C,2hrs. | 4.42 |
| RC-HB-DBM + 5% $Zr0_2$* | Sintered 1500°C,2hrs.<br>Sintered 1500°C,2hrs.+ | 5.76 |
| RC-HB-DBM + 5% $Zr0_2$ | HIP 1500°C,4hrs. | 6.57 |

* Results from (19).

The above results indicate that $ZrO_2$ addition improves the toughness of alumina and further improvement can be had by HIPing treatment. It is postulated that HIPing treatment to Alcoa 16 + 5%.$ZrO_2$ would further improve the toughness.

A comprehensive study is required for the optimization of density (thereby hardness), erosion rate and fracture toughness by controlling $ZrO_2$ content and thermal treatments (including HIPing).

## ACKNOWLEDGMENTS

The author gratefully acknowledges the financial support of EMR. The author would like to express his gratitude to Mr. H. Stillman, S. MacKay and W. Gillis of NSRFC for their assistance to carry out all experimental works, Dr. S. G. Whiteway and J. R. Wright of NRC ARL, Halifax for their advice and guidance in this project.

## REFERENCES


1. P. F. Becher and V. J. Tennery, "Fracture Toughness of $Al_2O_3$-$ZrO_2$ Composites," P383 on Fracture Mechanisms of Ceramics, Vol. 6., Edited by R. C. Bradt, A. G. Evans, D. P. H. Hasselman and F. F. Lange, Plenum Press, New York, 1983

2. E. C. Sabbarao, H. S. Maiti, and K. K., Srivastava, Phys. Stat. Sol. 21:9 (1974)

3. A. Heuer and G. L. Nord Jr., "Electron Microscopy in Mineralogy", H. R. Weuk, ed., Springer-Verlag, (1976), p. 274.

4. F. F. Lange, Research of Microstructurally Developed Toughening Mechanisms in Ceramics. Part 1: Size Effects Associated with the Thermodynamics of Constrained Transformations, Technical Report to Office of Naval Research, Contract No. N00014-77-C-0441 (1981).

5. A. G. Evans and A. H. Heuer, Transformation Toughening in Ceramics: Transformations in Crack-Tip Stress Fields, J. Am. Cer. Soc. 63:241 (1980).

6. F. F. Lange, Research of Microstructurally Developed Toughening Mechanisms in Ceramics. Part 2: Contribution to Fracture Toughness, Technical Report to Office of Naval Research, Contract No. N00014-77-C-0441 (1981).

7. F. F. Lange, Research of Microstructurally Developed Toughening Mechanisms in Ceramics. Part 4: Fabrication, Fracture Toughness and Strength of $Al_2O_3/ZrO_2$ Composites, Technical Report to Office of Naval Research, Contract No. N00014-77-C-0441 (1981).

8. F. F. Lange, J. Mat. Sci. 17, 247-54 (1982).

9. A. H. Heuer, N. Claussen, W. M. Kriven, M. Ruhle, J. Amer. Ceram. Soc. 65 642-650 (1982).

10. A. G. Evans, N. Burlingame, M. Drory, W. M. Kriven, Acta Metall. 29 447-456 (1981).

11. K. K. Srivastava, R. N. Patil, C. B. Chandary, K. V. G. K. Gokhole and E. C. Subbarao, Trans. Brit. Cerm. Soc. 73, 85 (1974).

12. G. G. Scott, J. Mat. Sci. 10. 1527 (1975).

13. V. S. Stubican, R. C. Hink and S. P. Ray, J. Amer. Ceram. Soc. 61, 17 (1978).

14. The Canadian Journal of Chemical Engineering, "Erosion and Termal Shock Tests on Ceramic Materials". S. G. Whiteway, E. W. Chan and A. Kazi.

15. Ruff, A. W. and Ives, L. K., "Measurement of Solid Particle Velocity in Erosive Wear", WEAR 35, 195-199 (1975).

16. Faber, Huang and Evans, "Quantitative Studies of Thermal Shock in Ceramics Based on Novel Techiques", J. Amer. Ceram. Soc. 64 (5), 296 (1981).

17. Munz, D., Bulsey, R. T., Shannon, J. L., "Fracture Toughness Determination of $Al_2O_3$ using Four-Point-Bend Specimens with Straight Through and Chevron Notches". J. Amer. Ceram. Soc. May-June 1980 Vol. 63, No. 5-6, p. 300-305.

18. J. H. Giovanola and D. A. Shockey, SRI International, Melno Park, CA. Fracture Mechanics of Ceramics Vol. 6. Edited by R. C. Bradt, A. G. Evans, D. P. H. Hasselman and F. F. Lange, Plenum Press, N.Y. 1983.

19. S. G. Whiteway, E. W. Chan, D. D. Morphy and A. Kazi, Resistance to Abrasion and Thermal Shock in Transformation Toughened Alumina. To be published in J. Can. Cera. Soc.

# APPENDIX A

## PHYSICAL PROPERTIES OF POWDER

## Properties of TSK-ZIRCONIA powder

### TZ - 3Y (Lot No. Z305207P)

1. Chemical Analysis

| | | |
|---|---|---|
| $Y_2O_3$ | 5.13 | wt% |
| $Al_2O_3$ | 0.100 | wt% |
| $SiO_2$ | 0.018 | wt% |
| $Fe_2O_3$ | 0.005 | wt% |
| $Na_2O$ | 0.006 | wt% |
| Ig.Loss | 0.8 | wt% |

2. Crystallite Size 240 A

3. Specific Surface Area 19 $m^2/g$

**ALUMALUX Alcoa Chemicals Division**
**High Purity Calcined Aluminas**

| Typical Chemical Analysis-PPM | Alumalux-39 $Al_2O_3$ 99.9% |
|---|---|
| $SiO_2$ | 100 |
| $Fe_2O_3$ | 100 |
| CaO | 50 |
| $Na_2O$ | 75 |
| $Ga_2O_3$ | 40 |
| Others | <50 |

**Typical Physical Properties**

| | |
|---|---|
| Surface Area $m^2/g$ | 3-6 |
| Ultimate Crystal Size | <0.5μ |

**Typical Ceramic Properties**

| | |
|---|---|
| Fired Density g/cc | 3.91 |
| Linear Shrinkage % | 18.0 |
| Fired One Hour at | 1540°C |

**REALOX Alcoa Chemicals Division**
**Calcined Aluminas**

| Typical Chemical Analysis Wt. Percent | A-16 |
|---|---|
| $Al_2O_3$ | 99.7 |
| $Na_2O$ | .08 |
| $SiO_2$ | .02 |
| $Fe_2O_3$ | .01 |
| MgO | .00 |
| CaO | .01 |
| $B_2O_3$ | .001 |

**Typical Physical Properties**

| | |
|---|---|
| Surface Area$^{(2)}$ $m^2/g$ | 3-6 |
| Ultimate Crystal Size - μm | <.5 |

**Typical Ceramic Properties**
**Ground to Ultimate Crystals**

| | |
|---|---|
| Fired Density g/cc | 3.91 |
| Linear Shrinkage % | 18.0 |
| Fired One Hour at | 1540°C |

## REYNOLDS CHEMICALS

### HIGH PURITY ALUMINA

### RC-HP DMB

**TYPICAL ANALYSIS**

**Chemical**

| | | | |
|---|---|---|---|
| $Al_2O_3$ | 99.95% | $Cr_2O_3$ | 0.0003% |
| $Na_2O$ | <0.008% | CuO | 0.0003% |
| $SiO_2$ | 0.016% | BeO | <0.0005% |
| $Fe_2O_3$ | 0.0038% | $Li_2O$ | 0.002% |
| CaO | <0.008% | $MoO_2$ | <0.001% |
| MgO | 0.05 | $P_2O_5$ | <0.001% |
| $TiO^2$ | 0.001% | $K_2O$ | <0.001% |
| $Ga_2O_3$ | 0.007% | C | <0.001% |
| MnO | <0.0005% | S | 0.0009% |

**Physical**

| | RC-HP DBM |
|---|---|
| Surface Area, $M^2$/gram | 6-8 |
| Alpha Alumina, % | 95 |
| Median Crystal Size, μm | 0.55 |

**Ceramic** Density: Fired: g/cc 3.96